

Coordination Bonding in Dicopper and Dichromium Tetrakis (μ -acetato)-diaqua Complexes: Nature, Strength, Length, and Topology

Michal Malček *,^[a] Barbora Vénosová,^[a] Ingrid Puškárová,^[a] Jozef Kožíšek,^[a] Marián Gall,^[b] and Lukáš Bučinský *^[a]

Geometry optimization, energetics, electronic structure, and topology of electron density of dicopper (I) and dichromium (II) tetrakis(μ -acetato)-diaqua complexes are studied focusing on the metal–metal interactions. The performance of broken symmetry (BS) single-determinant ab initio (Hartree–Fock, Møller–Plesset perturbation theory to the second and third orders, coupled clusters singles and doubles) and density functional theory (BLYP, B3LYP, B3LYP-D3, B2PLYP, MPW2PLYP) methods is compared to multideterminant ab initio (CASSCF, NEVPT2) methods as well as to the multipole model of charge density from a single-crystal X-ray diffraction experiment (Herich et al., *Acta Cryst.* 2018, B74, 681–692). In vacuo DFT geometry optimizations (improper axial water ligand orientation) are compared against the periodic ones. The singlet state is found to be

energetically preferred. J coupling of (I) becomes underestimated for all ab initio methods used, when compared to experiment. It is concluded that the strength of the direct M–M interactions correlates closely with the J coupling magnitude at a given level of theory. The double potential well character of (II) and of the dehydrated form of (II) are considered with respect to the Cr–Cr distance. The physical effective bond order of the metal–metal interaction is small (below 0.1 e) in (I) and moderate (0.4 e) in (II). The CASSCF results overestimate the electron density of the metal–metal bond critical point by 20% and 50% in (I) and (II), respectively, when compared to the multipole model. © 2019 Wiley Periodicals, Inc.

DOI: 10.1002/jcc.26121

Introduction

Metal–metal (M–M) interactions have raised a considerable attention since the discovery of $M_2(CO)_{10}$ complexes (where $M = Mn$ and Re).^[1] The carbonyls have been quickly extended by additional classes of complexes with direct M–M interactions such as halogenide ions like $[Re_2Cl_8]^{2-}$ for instance and double dentate ligands interconnecting the metal centers $[M_2L_4]$ or $[M_2L_2]$ such as carboxylate anions (although the group of bidentate ligands is considerably large and the coordination number depends on the ligand charge and the oxidation state of the central metal atom).^[2] Currently, the number of complexes that exhibit M–M interactions and/or bondings is huge, in the case of 3d homodimers (with M–M distance limited to 2.8 Å), the Cambridge Structural Database (version 5.40 2018) search yields 50, 101, 353, 149, 3231, 1342, 359, 1957, and 47 hits for Ti, V, Cr, Mn, Fe, Co, Ni, Cu and Zn, respectively, when no other metal is bonded to one of the metal atoms.* This is reflected in the revision of 3d homometallic M–M complexes of Lyngdoh et al.,^[2] summarizing the current state and general trends about the bond lengths and bond orders in the particular systems from an experimental and theoretical viewpoint. In addition, M–M interactions have been further reviewed from the stand point of the topology of electron density by Lepetit et al.^[3] As highlighted already in the second

edition of Cotton and Wilkinson's *Inorganic Chemistry Textbook*,^[4] the M–M distance (with respect to the covalent radius) can be regarded as a good measure of M–M bond strengths. In the presence of carboxylate anions, this range starts at weak interactions (formally a single bond) in Cu–Cu and reaches a multiple bond mode in Mo–Mo systems. Hence, the bond order within the M–M moiety ranges from a multiple bond mode in, for example, $[Re_2Cl_8]^{2-}$ or $[Mo_2(OOCR)_4]$ to only weak rather ligand bridge stabilized interactions in, for example, $[Cu_2(OOCR)_4]$. Other M–M moieties, such as Cr–Cr for instance, can be formally considered bonded in a multiple nature, albeit the physical criteria showed on a weak single bond.^[4] A further important point to mention (aside of a

[a] M. Malček, B. Vénosová, I. Puškárová, J. Kožíšek, L. Bučinský
Faculty of Chemical and Food Technology, Institute of Physical Chemistry and Chemical Physics, Slovak University of Technology in Bratislava, Radlinského 9, SK-812 37 Bratislava, Slovak Republic
E-mail: michal.malcek@stuba.sk or lukas.bucinsky@stuba.sk

[b] M. Gall
Faculty of Chemical and Food Technology, Institute of Information Engineering, Automation, and Mathematics, Slovak University of Technology in Bratislava, Radlinského 9, SK-812 37 Bratislava, Slovak Republic

Contract Grant sponsor: Agentúra na Podporu Výskumu a Vývoja; Contract Grant numbers: APVV-15-0053, APVV-15-0079; Contract Grant sponsor: Vedecká Grantová Agentúra MŠVVaŠ SR a SAV; Contract Grant numbers: 1/0466/18, 1/0598/16, 1/0718/19; Contract Grant sponsor: European Region Development Funds; Contract Grant number: 26230120002

© 2019 Wiley Periodicals, Inc.

*A simple structure search of any bond type between two metals lead to 48206 hits in the CSD database (version 5.40 2018) or 35724 when the bond distance is limited to 2.8 Å.

physical vs. formal oxidation state and thus physical bond order/effective bond order [EBO] and formal bond order) is the orbital framework used in the theoretical treatments which on the one hand is an almost mathematical necessity to obtain solutions in quantum mechanics of many electrons systems (more than one) and to gain a pictorial representation of a system studied. On the other hand an orbital is a mathematical tool, not a physical reality and can be considered as almost a bias with respect to an interpretation of, for example, bonding interactions upon the shape of canonical molecular orbitals (MOs). Still, the bond theory allows for a very practical rationalization of M–M bonding interactions with respect to the ordering and occupation of the $\sigma\pi\delta\delta^*\pi^*\sigma^*$ orbitals build as a linear combination of the metal d orbitals.^[3,5] Hence, the comparison between orbital-based approaches and density-based representations (topology of scalar fields derived from density and/or Kohn–Sham orbitals) is well suited to gain a compact, but not necessarily unified, characterization of bonding interactions. The large number of compounds with direct M–M interactions existing opens a great field of challenges and tasks for the theoretical treatment and description/characterization of these interactions. It is obvious that not all challenges and degrees of freedom can be accomplished in a single study. The compounds choice, presented herein, is motivated by the existence of experimental reference data available with respect to energetics and charge density, hence enabling a direct comparison of several (DFT and ab initio) levels of theory to experimental references.

We have chosen two isostructural complexes tetrakis(μ_2 -acetato)-diaqua-dicopper(II) [Cu₂(OAc)₄·2H₂O] and tetrakis(μ_2 -acetato)-diaqua-dichromium(II) [Cr₂(OAc)₄·2H₂O], abbreviated as (I) and (II), respectively. This work is a continuation of authors' previous experimental work of Herich et al.,^[6] which reports robust and compact multipole model of charge densities derived from single-crystal X-ray diffraction (SCXD) experiment of both compounds and hence can be used as a reference for the theoretical treatment of electron density and bonding characterization. The accurate experimental data^[6] include anisotropic correction for secondary extinction.^[7] The outcome of this reference experimental study^[6] can be summed up as follows: (1) there are only four classical coordination bonds M–O_{acetate}; (2) M–M interaction is an electrostatic one; (3) the M–O_{water} is merely an electrostatic interaction between the oxygen lone electron pair and the positive area of the M(II) ion (this conclusion was approved also by Scatena et al.^[8]). From the theoretical perspective, the static electron correlation effects are present in both of the chosen systems, hence it is reasonable to compare single-determinant versus multi-determinant treatments when considering the spin state and energetics due to the M–M (spin) interactions. Having experimentally derived charge density^[6] and energetics by means of *J* coupling (and/or singlet–triplet gap) values,^[9–13] one can critically review the performance of different theoretical methods for the treatment of the compounds chosen. To be mentioned in this respect as well, the pure homonuclear metallic dimers offered an exceptional meeting point of experiment and theory.^[2] The group 11 and 12 closed-shell dimers^[14–16] are a

further proof of the appropriateness of the theoretical treatment of dynamic electron correlation, the complete basis set limit extrapolations, the relativistic effects, and the basis set super position error with respect to the experimentally determined spectroscopic properties/constants. On the contrary, the group 6 dimers (in particular Cr₂)^[17–24] offered a challenge with respect to the multideterminant nature of the ground state, where even the DFT methods were successful in hitting the right position and depth of the Cr₂ potential well.^[25] Interestingly, the Cr₂⁺ cation is found stable according to Yamada et al.^[26] and similar is true for Cr₂²⁺.*

This study gives first a brief overview of works related to compounds (I)^[6,9–13,27,28] and (II)^[6,18,19,29–41] in the section “Overview of Previous Results.” The “Computational details” section compiles the state-of-the-art methods of computational chemistry employed to assess and describe the geometry, energetics, electronic structure, and bonding properties of the two coordination compounds studied. In the “Results” section, the in vacuo (complete active space [CAS], Hartree–Fock [HF], Møller–Plesset perturbation theory to the second order [MP2] and density functional theory [DFT]) geometry optimizations are compared to periodic DFT ones (including M–M potential energy surface [PES] scans at DFT and N-electron valence perturbation theory to the second order [NEVPT2] levels of theory) and to experimental results to shed light on the issues with M–M distances for the two compounds studied. The spin state preference (*J* coupling and/or singlet–triplet gap ΔE_{S-T}) of (I) is discussed, comparing DFT (B3LYP, BLYP, B3LYP-D3, B2PLYP, MPW2PLYP), ab initio single-determinant approaches (HF, MP2, Møller–Plesset perturbation theory to the third order [MP3], coupled clusters singles and doubles [CCSD]) as well as multideterminant (CAS and NEVPT2) approaches (using the experimental geometry of Herich et al.^[6]). In the case of (II), the CAS and NEVPT2 results are compared to HF, MP, and DFT spin states preferences, including *J* coupling assessment. Electronic structure is characterized by means of Löwdin atomic orbital (AO) populations and Wiberg's bond orders (WBOs), as well as quantum theory of atoms in molecules (QTAIM) analysis and electron localization function (ELF) visualization. Furthermore, the electronic configuration of the metal atoms is highlighted at various spin states and/or levels of theory. The structure of the studied paddle-wheel coordination compounds (I) and (II) is shown in Figure 1.

Overview of Previous Results

Compound (I)

The X-ray crystal structure of cupric acetate [Cu₂(OAc)₄·2H₂O] (I) has been determined for the first time by Niekerk and Schoening^[27] reporting the Cu–Cu dimer stabilized by four acetate ligands and a Cu–Cu distance of 2.64 Å. More recent studies have reported the Cu–Cu distance of 2.6107,^[28] 2.619,^[9]

*The Cr₂⁴⁺, Cu₂⁴⁺, and Cu₂²⁺ dimers are not stable (the interaction is repulsive) for high spin and a BS singlet UMP2/6–311++G** geometry optimizations. In the case of Cr₂²⁺ dimer the BS singlet UMP2/6–311++G** geometry optimization yields a value of 2.9058 Å.

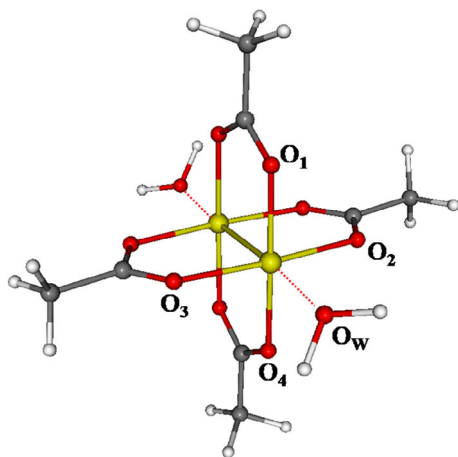


Figure 1. The visualization of the molecular structure and selected atoms labeling (where W = water) of studied compounds (I) and/or (II). [Color figure can be viewed at wileyonlinelibrary.com]

and 2.6108 Å^[6] in the same cupric acetate complex. Charge density of (I) has already been experimentally or theoretically studied by means of QTAIM analysis by Bertolotti et al.,^[28] Shee et al.,^[9] and Herich et al.^[6] Bertolotti et al.^[28] have taken into account the ROB3LYP/6-311++G** triplet states and the experimental geometry. It has been pointed out in Bertolotti et al.^[28] that the single-molecule (in vacuo) geometry optimization affects the bond distances with respect to the crystal structure, $\Delta_{\text{Cu}(1)-\text{O}(3)} = 0.065$, $\Delta_{\text{Cu}(1)-\text{O}(4)} = 0.047$, and $\Delta_{\text{Cu}(1)-\text{O}(5)} = 0.162$ Å. The QTAIM delocalization index (DI) between the copper atoms in (I) was 0.129 which indicates a low electron share.^[28] Shee et al.^[9] have used the BP86 functional and pseudopotentials for Cu atoms in (I) and $[\text{Cu}_2(\text{OAc})_4]$, the dehydrated form of (I). The found Cu–Cu Wiberg's bond indexes of Shee et al.^[9] show on a value smaller than one (actually 0.1 and 0.3 *e* for the basis set without and with diffuse functions, respectively). Furthermore, Shee et al.^[9] have shown that the water molecule in (I) becomes twisted in the optimized geometry, forming hydrogen bonds with the acetate oxygens. Jerabek et al.^[10] have reported DFT geometry optimizations of $[\text{M}_2(\text{OAc})_4]$, where M = Cu, Ag, and Au, and considered relativistic effects with respect to energetics (dissociation energies and *J* couplings), Löwdin atomic charges and ELF plots (the *J* coupling value in $[\text{Cu}_2(\text{OAc})_4]$ reported was -268 cm^{-1}).^[10] Kyuzou et al.^[11] have reported a susceptibility-based *J* coupling measurement of (I) and found a value of -298 cm^{-1} , which agrees with previous experimentally determined *J* coupling constants -286 ^[12] and -305 ^[13] cm^{-1} . Actually, Goodgame et al.^[13] have entitled their work "Insignificance of metal-metal bonding in antiferromagnetism of copper (II) carboxylate dimers" and assign the antiferromagnetism to a super exchange via the carboxylate bridges. Nevertheless, Shee et al.^[9] have performed a dependence of singlet–triplet energy gap on the Cu–Cu distance arguing that the acetyl bridge ligands are responsible for a ferromagnetic exchange, when taking into account that the singlet versus triplet ground-state preference switches at 2.9 Å. The UB3LYP/LANL2DZ *J* coupling value obtained in Kyuzou et al.^[11] is -295 cm^{-1} , albeit the theoretical value depends naturally on the basis set choice as

reported therein. Furthermore, Kyuzou et al.^[11] have explored the electronic transitions within the TD-DFT framework as well. Shee et al.^[9] have reported BP86 functional *J* couplings of larger magnitude for their optimized geometries (-497 cm^{-1}) in comparison with the already referenced values, *vide supra*.

Compound (II)

The X-ray crystal structure of chromium acetate $[\text{Cr}_2(\text{OAc})_4 \cdot 2\text{H}_2\text{O}]$ (II) has been determined for the first time also by Niekerk et al.,^[35] reporting the Cr–Cr distance of 2.64 Å. Cotton et al.^[36] have determined the metrically corrected Cr–Cr distance of 2.362 (1) Å in (II). The Cr–Cr bond length of (II) found in the latest experimental study of Herich et al.^[6] is 2.34779 Å, and which confirmed the previous X-ray structure of Cotton et al.^[36] Furthermore, the review of Lyngdoh et al.^[2] points out that the Cr–Cr bond length in the apically coordinated tetracarboxylates varies from 2.15 to 2.55 Å with respect to the apical bridging ligand (Cr–Cr bond lengths for the acetyl group are between 2.295 and 2.411 Å). Without any apical ligand, the experimentally determined Cr–Cr distance is 1.966 Å.^[37] The first theoretical electron density analysis of this complex has been performed at HF and CI levels of theory by Benard et al.^[38] for an experimentally determined Cr–Cr bond distance of 2.35 Å. However, it has to be mentioned, and the authors critically commented on the fact that the self-consistent field (SCF) calculations used therein do not provide a realistic picture of M–M interactions.^[38] Further theoretical geometry optimizations^[29,39–41] of the bare $[\text{Cr}_2(\text{OAc})_4]$ system have led to Cr–Cr bond distances between 2.40 and 2.50 Å (mostly restricted HF (RHF) configuration interaction (CF) or generalized valence bond (GVB) results were reported). The obtained GVB optimized Cr–Cr distance in (II) was 2.60 Å.^[29] Still, only little attention has been spent on the spin state preference and energetics in the aforementioned theoretical pilot studies of $[\text{Cr}_2(\text{OOCR})_4]$ like systems. Finally, Andersson et al.^[30] have reported a detailed DFT (BLYP, B3LYP), CASSCF, and CASPT2 study on the Cr–Cr bond lengths in $[\text{Cr}_2(\text{OOCR})_4]$ and $[\text{Cr}_2(\text{OOCR})_4 (\text{H}_2\text{O})_2]$ complexes (with R = H, CH₃). It has been shown that only in the case of the restricted DFT calculations, the $[\text{Cr}_2(\text{OOCR})_4]$ bond length becomes shorter (1.8 Å) when comparing to experiment (1.966 Å).^[37] Nevertheless, for the hydrated dimer $[\text{Cr}_2(\text{OOCH})_4 (\text{H}_2\text{O})_2]$, the restricted DFT value remained heavily underestimated (1.875 Å) in comparison with experiment (± 2.35 Å). On the contrary, the unrestricted DFT values of Cr–Cr bonds reported therein^[30] are overestimated in comparison with experiment for $[\text{Cr}_2(\text{OOCH})_4 (\text{H}_2\text{O})_2]$ by more than 0.1 Å. The CASPT2 Cr–Cr bond length was found to be 2.43 Å.^[30] In the work of Petrie and Stranger,^[31] the optimized Cr–Cr bond lengths are considerably shorter (around 2.0 Å) in $[\text{Cr}_2(\text{OOCH})_4]$ for all the DFT functionals employed, when using the unrestricted broken symmetry (BS) approach of Noodleman and Norman.^[32] A similar result was reported in Kitagawa et al.,^[18] who have

*CASSCF and CASPT2 geometry optimizations of $[\text{Cr}_2(\text{OOCH})_4]$ lead to longer bond lengths of about 2.85 and 2.54 Å, respectively. Nevertheless, the analysis of the inner and outer minimum in the Cr_2 dimer with respect to the treatment of 3s3p electron correlation lead to a correction of the inner minimum depth, which is used to explain the shift in the reported CASPT2 results of $[\text{Cr}_2(\text{OOCH})_4]$.

applied an approximate spin projection as well as the BS treatment, obtaining satisfactory Cr–Cr distances in the BLYP and B3LYP calculations of (II). Furthermore, Andersson et al.^[30] have reported for (II) the CASPT2 singlet–triplet gap of 983 cm⁻¹ which agrees excellently with the experimental value of 980 cm⁻¹.^[33] Roos et al.^[19] have characterized the Cr–Cr interaction in [Cr₂(OOCH)₄] as a formally quadruple bond with an EBO value of 2.0. The actual physical bond order in [Cr₂(carboxylates)₄] is reported to be below the formal bond order of four also in the DFT calculations.^[34]

Computational details

Experimental (X-ray) structures of (I) and (II) were taken from the previously published work of Herich et al.^[6]

In vacuo single-point calculations and geometry optimizations have been performed at the DFT (i.e., functionals BLYP,^[42,43] B3LYP,^[42–45] and B3LYP including the D3 version of Grimme's dispersion correction [GD3]^[46]), HF and MP2 levels of theory along with the 6-311G* basis set^[47,48] in Gaussian09 program package.^[49] In vacuo single-point calculations further included also for the double-hybrid B2PLYP^[50] and MPW2PLYP^[51] functionals, MP3 and CCSD levels of theory, with the active space chosen according to text, vide infra. In addition, 6-31G* and 6-311++G** basis sets are used for comparison purposes of the basis set quality impact on the DFT spin state energetics and DFT-optimized geometries (for the same reasons, the def2-TZVP^[52] basis set has been utilized as well). Restricted (closed shell) and unrestricted high spin as well as BS^[53–57] approaches have been used to study the different spin multiplets of (I) and (II) systems. In the case of the BS calculations, original unrestricted energies are shown, without any corrections or further manipulations. Note also that methods denoted unrestricted (U), like UBLYP for instance, denote implicitly a BS calculation for lower than maximum multiplicity case targeting the antiferromagnetic coupling.

The energy difference between the unrestricted triplet and singlet states (corresponding to minus J coupling) can be evaluated in several ways. The “bare” triplet (M3)–singlet (M1) energy gap $\Delta E_{U,M3-M1}$ can be evaluated according to

$$\Delta E_{U,M3-M1} = -J = (E_{M3} - E_{M1}), \quad (1)$$

This is derived with respect to the spin Hamiltonian^[58] $H_S = -J S_A S_B$, where the individual energy levels are given by $E_S = -(J/2)[S(S+1) - S_A(S_A+1) - S_B(S_B+1)]$. These can be further shifted to $E_S = -(J/2)[S(S+1)]$, where for the singlet–triplet gap the factor of one half and the $S(S+1)$ value of two do cancel out ($\Delta E_{U,M3-M1} = -J$).

The energy gap in the BS calculations (abbreviated as $\Delta E_{BS1,M3-M1}$), where the spin contamination may affect significantly the overall energetics, can be evaluated according to the following formula^[53,59,60]:

$$\Delta E_{BS,M3-M1} = -J = 2(E_{M3} - E_{BS,M1}) / (\langle S^2 \rangle_{M3} - \langle S^2 \rangle_{BS,M1}), \quad (2)$$

where E_{M3} denotes the unrestricted high spin (triplet) energy. The particular $\langle S^2 \rangle$ expectation values of (I) and (II) are

compiled in Supporting Information Table S1. This equation can be made also related to the work of Caballol et al.^[60] who have obtained the following equation:

$$-J = 2(E_{M3} - E_{BS,M1}) / (1 + S_{ab}^2), \quad (3)$$

where S_{ab} is the overlap between magnetic orbitals (being an approximation of the overlap between two BS wave functions $|\dots ab\rangle$ and $|\dots a\bar{b}\rangle$). One also has to mention that the two magnetic orbitals have to be well defined (i.e., small-spin polarization of the closed-shell orbitals). Caballol et al.^[60] have mentioned two limiting values of S_{ab} namely 0 (strong orthogonal or localized limit) and 1 (delocalized limit). The character of the open-shell orbital and the polarization of closed-shell orbitals are discussed in the “Results” section.

Additional in vacuo calculations (both single points and geometry optimizations) were carried out at the CAS self-consistent field^[61–63] level of theory, without including the resolution of identity approximation,^[64] in ORCA software package (version 4.0.1.2).^[65] The CAS was built of the d-like orbitals of the two metal centers. The number of correlated electrons was 18 and 8 in the case of (I) and (II), respectively. Hence, the CAS-labeled calculations are the shortcuts for CASSCF (18,10) and CASSCF (8,8) in the case of (I) and (II), respectively. In the case of (II), the smaller active space has been chosen, because of the presence of intruder states in the singlet-state calculations, although the energetics of the CASSCF (8,10) calculations of (II) is also considered. Furthermore, NEVPT2^[66–69] level of theory has been utilized to account for the dynamic electron correlation in the single-point CAS calculations (the active space included valence electrons and 3s and 3p electrons of the metal atoms). In addition, a NEVPT2 PES scan has been performed for the Cr–Cr and Cu–Cu bond lengths (with keeping the water molecules in a constant position with respect to the central atom). These PES calculations have been performed for (I) and (II) as well as for the dehydrated form of (II).

Periodic (crystal phase) single-point calculations and geometry optimizations have been performed in the CRYSTAL17^[70,71] program package using BLYP and B3LYP functionals and the pob-DZVP basis set.^[72] Periodic geometry optimizations have been done for atomic positions only (ATOMSONLY).

QTAIM analysis^[73] has been performed in the AIMAll package^[74] for every system under study using the Gaussian09 checkpoint and/or ORCA wavefunction (wfn) files. The ORCA wfn files have been produced via the Molden2AIM utility software.^[75] TOPOND software^[76] has been used in the QTAIM calculations of periodic systems as included in CRYSTAL17. The QTAIM method is employed to evaluate charge and spin densities at the particular atoms (basins) and to estimate the character of the interatomic interactions via properties in the bond critical points (BCPs) and via DIs. ELF^[77] is inspected in the “spin-polarized” formalism,^[78] via the DGrid^[79] and MULTI-WFN^[80] packages, to pictorially identify the presence of M–M interactions in the systems studied. It is important to mention that the one electron density matrix approximation of Müller^[81] is actually utilized in the case of DIs evaluated upon the CAS

natural orbitals. Limits for the missing two electron reduced density matrix contributions in covalently bonded model molecules are discussed in Francisco et al.^[82] A similar study for electron localization indices is also reported.^[83,84] Francisco et al. have shown that the DI value of N₂ molecule changes from 3.042 at HF level of theory to 1.988 at the CAS(10,10) one. On the contrary, Fradera et al.^[85] have reported a CI value of 2.219 and in the our case CAS(10,10)/6-311G* level of theory yields a value of 2.297 when the analysis is based on the natural orbital populations in the wfn file and/or on the usage of the one electron reduced density matrix approximation. Still, this approximation seems to be qualitatively meaningful and the DIs obtained here are in good agreement when compared to unrestricted Hartree-Fock (UHF) or DFT results, *vide infra*.

To elucidate the electronic structure and/or the M–M interactions in the studied complexes also in the AOs perspective (although being thus more sensitive to the basis set choice), Löwdin populations and WBOs (calculated using ORCA package or MULTIFN software in cases of WBOs below 0.05) are reported. Visualization of the molecular structure, orbitals, and spin densities has been performed in the Molekel^[86] software suite with the isovalue set to ± 0.02 and ± 0.005 a.u., respectively; ELF 3D plots have been visualized with a 0.4 isovalue. ELF 2D plots have been visualized in the XCrySDen package.^[87,88]

Results and Discussion

Structural parameters from geometry optimization

Compound (I). The calculated bond distances and angles obtained from geometry optimizations are compiled in Table 1. One can see from Table 1 that in the case of (I), the closest agreement with the experimental values is provided by the UMP2 method. The UMP2 Cu–Cu distance of 2.610 Å reported herein corresponds well with the X-ray structure of Herich et al.^[6] 2.6108 Å. In addition, the potential energy scan with respect to change of the Cu–Cu distance performed at the NEVPT2 level of theory provides a very good agreement with the X-ray structure as well, see Table 1 and Supporting Information Figure S1a. Moreover, deviations between the DFT (both UB3LYP, UBLYP) and X-ray Cu–Cu bond lengths are below 0.1 Å for the in vacuo 6-311G* calculations (the hybrid UB3LYP functional underestimates the Cu–Cu distance less than the nonhybrid UBLYP one). The obtained Cu–Cu bond lengths are well in line with the previously published DFT results, see Table 1.^[9,18,28] On the other hand, the BS singlet UHF (or CAS) method fails in the case of Cu–Cu bond distance, leading to a value of 3.08 Å (or 2.84 Å for CAS), when compared to experiment,^[6] see Table 1.

The Cu–O₁₋₄ bond lengths become overestimated by max. 0.02 and 0.05 Å in the in vacuo UMP2 and DFT calculations, respectively, when compared to the X-ray structure.^[6] In the case of Cu–O_w bond lengths are the deviations with respect to X-ray experiment larger than in the case of Cu–O₁₋₄ bond and reach up to 0.2 Å. The obtained Cu–O₁₋₄ and Cu–O_w bond lengths agree well with the previously published DFT results,

see Table 1.^[9,18,28] The large Cu–O_w bond length deviation is closely related to changes of Cu–Cu–O_w angles, see Table 1. The in vacuo optimized Cu–Cu–O_w angle is more bent (except for CRYSTAL17 calculations) with respect to the experimental one, that is, $\pm 160^\circ$ versus 173° , respectively. This bending of the Cu–Cu–O_w angle is caused by the creation of two hydrogen bonds of the water hydrogens and the acetate oxygens in the in vacuo optimizations as shown previously in Shee et al.^[9] and grossly affects the obtained Cu–O_w bond lengths. In the case of the periodic calculations carried out in the CRYSTAL17 program code, the calculated and the experimental X-ray Cu–Cu–O_w angles are in close agreement (the difference is less than 0.5%), see Table 1. In the case of the periodic optimization of the triplet state, the UB3LYP functional performs very well with respect to the obtained Cu–Cu and Cu–O bond lengths when comparing to the experimental values, albeit a DZ quality basis set has been employed (only atomic positions were optimized). Results of 6-311++G** and 6-31G* in vacuo UB3LYP geometry optimizations are compiled in Table 1. The Cu–Cu bond distance improves for the UB3LYP/6-311++G** basis set with respect to the experimental geometry^[6] while the Cu–O distances became longer than for the 6-311G* geometry optimization. The 6-31G* basis set has been utilized for a consistency check of the smaller pob-DZVP basis set used in the CRYSTAL17 calculations.

Compound (II). The optimized CAS (for all multiplicities) and UBLYP/UB3LYP/UHF/UMP2 bond distances and angles of (II) are also presented in Table 1. In the case of the single-determinant optimizations of (II), only the high-spin state M9 and the energetically preferred BS singlet spin state M1 have been taken into account. All the theoretical methods based on the nonet (M9) multiplicity overestimate the experimentally obtained Cr–Cr bond distance (2.348 Å),^[6] including periodic geometry optimizations in CRYSTAL17. The calculated M9 Cr–Cr distances are within the interval of 2.7–3.0 Å, see Table 1. On the contrary, the singlet (M1) spin states lead to a considerable improvement of the Cr–Cr distances. The best agreement with the experiment is obtained for the M1 state at the UB3LYP level of theory (2.49 Å) and for the NEVPT2 PES scan of the Cr–Cr distance (2.43 Å), while the UBLYP functional considerably underestimates this distance (1.95 Å), see Table 1, Figure 2a, and Supporting Information Figure S1b. BS UHF and CAS results of (II) are close to each other and the UMP2 geometry optimization leads to shorter (yet overestimated) Cr–Cr distance with respect to UHF (experiment). In general, the obtained results correspond well with previously reported findings of Andersson^[30] and Kitagawa.^[18] Furthermore, the dehydrated form of (II) yields the following Cr–Cr bond lengths: 2.43 and 1.85 Å for the M1 UB3LYP and UBLYP, respectively (see Fig. 2b). In the case of NEVPT2, the double well of the PES scan of the dehydrated form of (II) is more troublesome to be addressed accurately. The inner potential well preference in the NEVPT2 PES of the dehydrated form of (II) was assessed in the case of UBLYP relaxed geometry (with the frozen experimental Cr–Cr distance), see Figure 2b, black solid line. Furthermore, we have to highlight the CASPT2 results of Andersson et al.^[30] who have

Table 1. Comparison of calculated optimized and experimentally obtained (X-ray) structural parameters (bond distances in Ångström and angles in degrees) of the studied systems (I) and (II), where subscripts W and 1–4 follows the notation in Figure 1.

System	Distances (Å)			Angles (°)
(I)	Cu—Cu	Cu—O _W	Cu—O _{1–4}	Cu—Cu—O _W
UBLYP	2.530 ^{M1} , 2.525 ^{M3}	2.324 ^{M1} , 2.321 ^{M3}	2.005 ^{M1} , 2.006 ^{M3}	158.79 ^{M1} , 159.38 ^{M3}
UB3LYP	2.585 ^{M1} , 2.571 ^{M3}	2.264 ^{M1} , 2.258 ^{M3}	1.981 ^{M1} , 1.980 ^{M3}	159.06 ^{M1} , 159.54 ^{M3}
UBLYP ^[a]	2.624 ^{M3}	2.130 ^{M3}	2.019 ^{M3}	173.85 ^{M3}
UB3LYP ^[a]	2.696 ^{M3}	2.112 ^{M3}	1.994 ^{M3}	173.33 ^{M3}
UB3LYP ^[b]	2.605 ^{M1} , 2.601 ^{M3}	2.299 ^{M1} , 2.298 ^{M3}	1.999 ^{M1} , 1.999 ^{M3}	163.93 ^{M1} , 163.80 ^{M3}
UB3LYP ^[c]	2.571 ^{M1} , 2.561 ^{M3}	2.250 ^{M1} , 2.271 ^{M3}	1.951 ^{M1} , 1.959 ^{M3}	158.49 ^{M1} , 158.41 ^{M3}
UHF	3.082 ^{M1} , 2.811 ^{M3}	2.121 ^{M1} , 2.201 ^{M3}	2.049 ^{M1} , 2.006 ^{M3}	146.02 ^{M1} , 161.57 ^{M3}
UMP2	2.610 ^{M1} , 2.610 ^{M3}	2.189 ^{M1} , 2.188 ^{M3}	1.953 ^{M1} , 1.954 ^{M3}	163.24 ^{M1} , 163.26 ^{M3}
CAS ^[d]	2.837 ^{M1} , 2.838 ^{M3}	2.197 ^{M1} , 2.197 ^{M3}	2.008 ^{M1} , 2.008 ^{M3}	160.73 ^{M1} , 160.68 ^{M3}
NEVPT2 ^[e]	2.611 ^{M1} , 2.611 ^{M3}	–	–	–
Relevant published data				
BP86 ^[f]	2.619 ^{M1}	2.378 ^{M1} , 2.366 ^{M1}	2.000 ^{M1}	
ROB3LYP ^[g]	2.678 ^{M3}	2.309 ^{M3}	2.014 ^{M3}	
X-ray ^[h]	2.61082(3)	2.14884(8)	1.9679	173.97
X-ray ^[i]	2.6107(4)	2.1474 (9)	1.9670	
(II)	Cr—Cr	Cr—O _W	Cr—O _{1–4}	Cr—Cr—O _W
UBLYP, M9	2.809	2.405	2.063	150.65
UB3LYP, M9	2.817	2.369	2.059	150.75
UBLYP, M9 ^[a]	2.878	2.164	2.069	171.19
UB3LYP, M9 ^[a]	2.902	2.180	2.064	170.65
UBLYP, M1	1.946	2.492	2.036	162.91
UB3LYP, M1	2.486	2.367	2.039	157.43
UBLYP, M1 ^[b]	2.227	2.459	2.040	166.28
UB3LYP, M1 ^[b]	2.522	2.394	2.042	162.24
UHF, M9	2.924	2.373	2.101	153.57
UMP2, M9	2.815	2.329	2.060	152.41
UHF, M1	2.847	2.375	2.095	155.17
UMP2, M1	2.656	2.323	2.048	156.67
CAS, M9 ^[d]	2.950	2.372	2.099	154.06
CAS, M7 ^[d]	2.918	2.372	2.097	153.73
CAS, M5 ^[d]	2.890	2.373	2.094	154.09
CAS, M3 ^[d]	2.868	2.374	2.093	154.42
CAS, M1 ^[d]	2.858	2.371	2.092	154.64
NEVPT2, M1 ^[e]	2.433	–	–	–
NEVPT2, M9 ^[e]	2.774	–	–	–
UBLYP, M1 ^[e]	2.057	–	–	–
UB3LYP, M1 ^[e]	2.497	–	–	–
Relevant published data				
UBLYP	2.347, ^[j] 2.224 ^[k]	2.281, ^[j] 2.342 ^[k]	2.018 ^[j] , 2.017 ^[k]	
UB3LYP	2.543, ^[j] 2.478 ^[k]	2.183, ^[j] 2.215 ^[k]	2.023 ^[j] , 2.021 ^[k]	
X-ray ^[h]	2.34779(8)	2.25798(11)	2.018	175.74
X-ray ^[i]	2.362(1)	2.272(3)	2.0179	

In the case of the Cu—O_{1–4} bond, average values are presented. Basis set used is 6-311G* unless stated otherwise and M stands for multiplicity.

[a] Calculations carried out in CRYSTAL17 using pob-DZVP basis set.

[b] 6-311++G** basis set used.

[c] 6-31G* basis set used.

[d] Calculations carried out in ORCA using 6-311G* basis set.

[e] Only M—M distance has been varied (the water molecules are kept in the same position with respect to M as in the experimental geometry).

[f] Values taken from LACVP*(Cu)/6-311++G*(rest) BS calculations of Shee et al.^[9]

[g] Values taken from 6-311++G** calculations of Bertolotti et al.^[28]

[h] Experimental values taken from Herich et al.^[6]

[i] Experimental values taken from Bertolotti et al.^[28]

[j] Values taken from 6-311+G* BS calculations of Kitagawa et al.^[18]

[k] Values taken from 6-311+G* approximate spin projection calculations of Kitagawa et al.^[18]

[l] Experimental values taken from Cotton et al.^[36]

very precisely addressed the necessity of the usage of 3s and 3p orbitals as a part of the PT2 active space. It is noteworthy, that also in the case of the copper acetates, the M—M distance becomes shortened after removal of the water ligands.^[8] Hence, one can conclude that the axial water ligands polarize the metal atom electron density toward the neighboring metal, what in turn enhances the M—M repulsion when water molecules are present in the axial positions. From an orbital

perspective, the antibonding interactions are stabilized (and bonding interaction are destabilized) in the presence of the apical ligand.

The Cr—O bonds and water ligand orientations (see Table 1) become altered for the optimized geometries of (II) in a similar fashion like in the case of (I), except that in the periodic calculations the Cr—O_W bond length becomes significantly shortened. Nevertheless, this Cr—O_W bond shortening is due to the

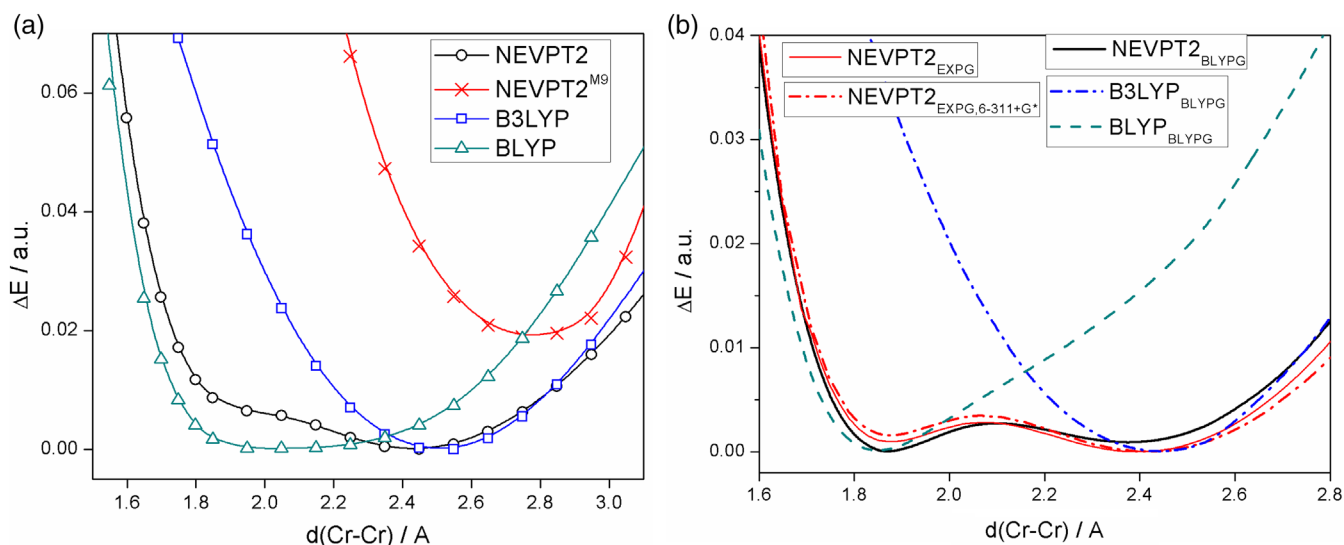


Figure 2. Relative NEVPT2 and DFT energies (ΔE) in a.u. with respect to the change of Cr–Cr distance: a) compound (II), b) dehydrated form of compound (II). Basis set used is 6-311G* and multiplicity is 1 unless stated otherwise. Abbreviations in subscripts EXPG and BLYPG stand for experimental^[6] and BLYP relaxed geometry, respectively. [Color figure can be viewed at wileyonlinelibrary.com]

overestimated Cr–Cr distance in the unchanged unit cell (only atomic positions were optimized). Still the Cr–Cr–O_W angle and the water coordination is in accordance with the experimentally obtained one for the periodic geometry optimization, while the calculated Cr–Cr–O angles in the in vacuo single-molecule calculations are again reoriented with hydrogens toward the oxygens of the acetate as in the case of (I). One can also see that the monitored UBLYP and UB3LYP distances and angles of (II) are strongly affected by the choice of the basis set, when comparing the particular 6-311G* and 6-311++G** values in Table 1.

Spin states preference

Compound (I). The CAS(18,10) and the particular NEVPT2 energies based on the experimental geometry of Herich et al.^[6] of the triplet and singlet ground states of (I) are compared to the unrestricted triplet and BS singlet as well as to restricted open-triplet and restricted singlet calculations at the DFT, HF, MP2, MP3, and CCSD levels of theory, see Table 2. The unrestricted BS singlet spin state calculations are found to be energetically preferred over the triplet spin state in the ab initio and DFT single-determinant calculations, see Table 2. This is in accordance with the CAS and the subsequent NEVPT2 calculations. Thus, the poor man's BS approach is indeed able to provide a qualitatively meaningful representation of the energetics of a wave function with two closely degenerate open shells of (I).

The low spin (singlet) versus high spin (triplet) energy gap is almost identical for the UHF and CAS levels of theory, ca. 20 cm⁻¹ without considering any correction of the BS treatment (i.e., $\Delta E_{U,M3-M1} = E_{U,M3} - E_{U,M1}$). The inclusion of dynamic electron correlation within the ab initio framework leads to a larger singlet–triplet energy gap $\Delta E_{U,M3-M1}$, see Table 2. The single-reference MP2 and MP3 calculations (valence electrons active) give values of 42 and 33 cm⁻¹, respectively. In the

shrunk active space (vide infra), the single-reference MP3 and CCSD values are 36 and 85 cm⁻¹, respectively. In the case of the NEVPT2 calculation, the $\Delta E_{U,M3-M1}$ is above 70 cm⁻¹ for the larger active space (with 3s and 3p electrons of Cu accounted for), see also the particular comments of Table 2. The same extension of the active space in the MP2 case shifts $\Delta E_{U,M3-M1}$ by ca. 20 cm⁻¹ up, while for MP3 by ca. 3 cm⁻¹ down. The MP3 and CCSD calculations have been performed especially because of the failure of the MP2 method which identifies the restricted closed-shell singlet spin state as the ground state (albeit the unrestricted MP2 $\Delta E_{U,M3-M1}$ is assessed correctly, i.e., singlet being below triplet).^{*} Nevertheless, it has to be noted that the ab initio (UCCSD, UMP2, UMP3, or NEVPT2) J values are underestimated in comparison with the experiment when using just the direct energy difference of eq. 1, see Table 2. This can be assigned to an overestimated localization of spin on the copper atoms and/or the underestimated metal–ligand interactions in contrast to experiment and/or DFT (see also spin density plots in Supporting Information Fig. S2 or the AO populations and QTAIM analysis in the following sections). The almost equal and underestimated ΔE_{M3-M1} values at UHF and CAS levels of theory (or MP vs. NEVPT2) show on an equal spin localization on the metal atoms in each case, vide infra. To improve the CAS and NEVPT2 values, the Cu–O interactions need to be accounted for in the CAS active space. It is also worth to point out that in the UHF regime, the BS open shells can be hardly identified laying deep in the orbital sea (for further detail see the following section and Supporting Information). Hence, there is a large (huge) spin polarization of the closed shells, and the

^{*}MP3 and CCSD calculations identify the unrestricted BS singlet spin state as the ground state again (as found in the HF, DFT, and CAS/NEVPT2 calculations). The failure of the MP2 single reference method seems to be further manifested in the NEVPT2 calculations which identify high CAS roots as a ground states, the particular NEVPT2 energies are compiled in Supporting Information Table S2.

Table 2. Relative energies for experimental (X-ray) structures of (I), where ΔE_{BS} corresponds to BS treatment according to eq. 2, and ΔE_U corresponds to uncorrected triplet-singlet values (eq. 1).

(I)	$\Delta E_{BS,M3-M1}$	$\Delta E_{U,M3-M1}$	$\Delta E_{(R-U),M1}$	$\Delta E_{(RO-U),M3}$
UBLYP	937.3	517.3	2382.3	182.5
UBLYP ^[a]		643.5	5383.4	–
UB3LYP ^[b]	396.2	199.9	11998.2	406.6
UB3LYP ^[a]		192.7	16983.2	–
UB3LYP ^[c]	399.1	201.4	11931.8	407.7
UB3LYP ^[d]	456.2	230.7	11023.9	440.2
UB3LYP ^[e]	371.4	187.2	12808.8	353.2
UB3LYP ^[f]	435.7	220.9	11407.7	561.7
UB2PLYP	226.2	113.0	–8195.1	605.0
UmpW2PLYP	201.1	100.2	–2759.1	636.8
UHF	41.6	20.7	77523.8	1194.1
UHF ^[f]	41.7	20.8	78174.0	1843.4
UMP2	84.9	42.2	–44154.3	777.4
UMP2 ^[f]	85.4	42.5	49206.6	1199.6
UMP3	66.0	32.8	27899.2	780.3
UMP2 ^[g]	124.7	62.0	–55243.6	–15.9
UMP3 ^[g]	58.4	29.0	47090.5	178.7
UMP3 ^[h] (51,–96)	72.2	35.9	20893.5	774.3
UCCSD ^[h] (51,–96)	170.2	84.7	14540.5	564.8
CAS		19.2, ^[i] 22.6, ^[j] 16.1 ^[k]		
CAS ^[f]		18.6, ^[i] 21.9, ^[j] 15.6 ^[k]		
NEVPT2 ^[g]		72.6, ^[i] 45.2, ^[j] 39.7 ^[k]		
NEVPT2 ^{[f], [g]}		73.3, ^[i] 43.2, ^[j] 46.3 ^[k]		
Relevant published data		268, ^[l] 298, ^[m] 295, ^[n] 286, ^[o] 497 ^[p]		

6-311G* basis set was used (unless stated otherwise). All the ΔE values are in cm^{-1} . Subscripts U, R, and RO refer to unrestricted, restricted, and restricted open, respectively.

[a] Periodic pob-DZVP calculation.

[b] Grimme's GD3 correction gave exactly the same ΔE values as the original B3LYP functional.

[c] 6-311G** calculation.

[d] 6-311++G** calculation.

[e] 6-31G* calculation.

[f] def2-TZVPP calculation.

[g] Active orbitals space accounts for the 3s3p (29,0) orbitals of Cu.

[h] Active orbitals space has been shrunk from (37,0) to (51,–96), that is, the (51, –96) energy window employs active orbitals in the range from –0.9 to 5.0 Eh, see Gaussian09 manual.

[i] Difference of lowest energy singlet and triplet CAS solutions.

[j] The triplet multiplicity lowest energy state solution has been expanded in the basis set of the singlet ground-state CAS solution.

[k] The singlet multiplicity ground state solution has been expanded in the basis set of the lowest energy triplet CAS solution.

[l] $|J|$ value taken from Jerabek et al.^[10]

[m] Experimental $|J|$ value taken from Kyuzou et al.^[11]

[n] Calculated DFT/LANL2DZ $|J|$ value taken from Kyuzou et al.^[11]

[o] Experimental $|J|$ value taken from Figgis et al.^[12]

[p] Calculated BP86 $|J|$ values taken from Shee et al.^[9]

original assumptions of Caballol et al.^[60] are not fulfilled. Still, when applying the correction given in eq. 2, naturally, the obtained $\Delta E_{BS,M3-M1}$ values become larger by a factor of two which shifts UCCSD, UMP2, and UMP3 estimates closer to experimentally determined J values, this is because the ab initio BS M1 (S^2) are actually equal to one (see the BS (S^2) expectation values compiled in Supporting Information Table S1), that is, overall one α open shell in total does not find the spatial overlap within the β spin counterpart, vide infra.

On the contrary, DFT calculations show that the nonhybrid (pure XC) UBLYP functional yields the largest $\Delta E_{U,M3-M1}$ gaps of about 500 cm^{-1} , while the hybrid UB3LYP functional $\Delta E_{U,M3-M1}$ gap values are around 200 cm^{-1} . The UB3LYP $\Delta E_{U,M3-M1}$ gap evaluated according to eq. 1, is in agreement with the previous theoretical $\Delta E_{U,M3-M1}$ gaps and/or experimental J values, see Table 2.* The UBLYP $\Delta E_{U,M3-M1}$ gap evaluated according to

eq. 1 is overestimated by a factor of two when compared to experimental J values (this is a general feature of pure GGA functionals,^[9] with a preference of the low spin states). The MP2-based double hybrids (UB2PLYP and UmpW2PLYP) yield $\Delta E_{U,M3-M1}$ values of around 100 cm^{-1} (albeit the double hybrids identify the restricted closed shell as the ground state as MP2 itself did, see Table 2). The usage of eq. 2 would shift the UB3LYP (or UBLYP) $\Delta E_{BS,M3-M1}$ values up by a factor of two (or four) which is not correct. Still, eq. 2 would lead to an improved agreement with experimental J values in the case of double hybrids (UB2PLYP and UmpW2PLYP). The comparison of results obtained for the chosen Pople style triple zeta basis set with the Ahlrichs def2-TZVPP basis set does not show any quantitative differences with respect to the obtained energetics, aside the case of $\Delta E_{(RO-U)}$, where the number of basis set functions is proportional to the energy (RO – U) difference, see Table 2. For completeness, NEVPT2 energies of (I) are provided in Supporting Information Table S2.

*Here, we omit the minus sign for the antiferromagnetic interaction (singlet below triplet state).

The periodic calculations have been performed to consider the crystal environment effects and possible contact interactions between the molecular moieties with respect to the spin states preference. Note that the actual unit cell contains 4 molecules (each formally possessing four possible combinations: $\alpha\alpha$, $\alpha\beta$, $\beta\alpha$ and $\beta\beta$), hence there are 128 unique spin state configurations (S_z projections) out of 256 possible, when assuming that the full spin inversion leads to double degeneracy (e.g. all α vs. all β) and when enforcing C_1 symmetry to be able to assess the full control over the BS unrestricted spin flips in the CRYSTAL17 package. The UBLYP/pob-DZVP energies yield the following nonet:septet: pentet:triplet:singlet degeneracy 8:32:48:32:8 with energies of 2561.2, 1924.1, 1283.6, 643.5, and 0.0 cm^{-1} (relative to the lowest BS singlet spin state). In the case of B3LYP/pob-DZVP level of theory these configurations yield the following energies: 769.6, 577.5, 385.1, 192.7, and 0.0 cm^{-1} for the particular nonet, septet, pentet, triplet, and singlet spin states, respectively. Hence, the periodic results are in a reasonable agreement with the in vacuo $\Delta E_{U,M3-M1}$ DFT values (compared with the DZ basis set quality 6-31G* results presented in Table 2).

Compound (II). The singlet is identified as the energetically lowest (ground) state of compound (II) at the CAS and NEVPT2 levels of theory, see Table 3. The multideterminant approaches

show the (relative) total energies to be proportional to the multiplicity ($E_S = -(J/2)[S(S+1)]$). The obtained NEVPT2 singlet-triplet gap is in agreement with the CASPT2 result of Andersson et al.^[30] (983 cm^{-1}) and the experimental value of 980 cm^{-1} of Cotton et al.^[33] On the contrary, the obtained DFT, UHF, UMP2, and UMP3 energies are oscillatory, see Table 3. Still, the BS unrestricted calculations do correctly assess the M1 ground state and the BS $\Delta E_{BS,M9-M1}$ energy differences, according to eq. 2, are in a qualitative accordance with the CAS and NEVPT2 results. The UHF approach underestimates the ΔE_{M9-M1} energy gap by a factor of two when compared to CAS, while the J coupling is underestimated only by less than 20%, when taking into account BS correction of eq. 2. The UMP2 and UMP3 do underestimate the NEVPT2 ΔE_{M9-M1} value by about 30%, and the J coupling is underestimated (BS correction of eq. 2) only by 10% again. UBLYP and UB3LYP overestimate the ΔE_{M9-M1} value and J coupling according to eq. 2 is overestimated by a factor of two and one half, respectively. The def2-TZVPP basis set results are very close to the 6-311G* basis set ones. As already found for (I) the solid-state CRYSTAL17 calculations yield UBLYP and UB3LYP $\Delta E_{BS,M9-M1}$ values which are in a reasonable agreement with the in vacuo calculations, see Table 3. In the case of (II), the spin is well localized at the metal centers, which is reflected in the agreement of NEVPT2 results (as well as

Table 3. Relative energies (relative to M1) of the experimental (X-ray) structure of (II) and J coupling estimates.

ΔE (II)	M1	M3	M5	M7	M9
CAS ^[a]	0.0	726.6	2015.9	4156.3	8434.0
CAS ^[b]	0.0	657.1	2005.6	4157.8	10285.0
CAS ^[c]	0.0	561.0	1699.7	3470.8	6064.3
CAS ^{[b], [d]}	0.0	665.3	2032.7	4224.6	7736.3
CAS ^{[c], [d]}	0.0	552.2	1674.3	3423.6	5995.4
NEVPT2 ^[a]	0.0	995.3	4270.2	7385.4	10722.5
NEVPT2 ^[b]	0.0	871.5	2652.1	5506.6	10285.0
NEVPT2 ^[c]	0.0	828.3	2514.7	5178.9	9314.7
NEVPT2 ^{[b], [d]}	0.0	886.0	2697.2	5611.4	10605.5
NEVPT2 ^{[c], [d]}	0.0	836.2	2540.6	5238.7	9471.4
UHF	0.0 (70987.0) ^[e]	17186.9	21920.3	15726.9	4919.5
UHF ^[d]	0.0	16290.8	20503.9	14862.6	4828.8
UBLYP	0.0 (14548.1) ^[e]	9069.8	12001.2	8503.8	17522.0, 18594.2 ^[f]
UB3LYP	0.0 (44373.4) ^[e]	11358.7	14376.6	9212.7	12563.3, 12815.7 ^[f]
UB3LYP ^[d]	0.0	11067.9	14167.7	9057.8	12463.4
UMP2	0.0 (59747.0) ^[e]	15422.1	19912.7	13677.7	6854.4
UMP2 ^[d]	0.0	14260.5	18372.6	12661.0	6906.9
UMP3	0.0 (60060.6) ^[e]	15177.6	19643.5	13848.7	6860.3
J (II)	M1	M3	M5	M7	M9
CAS ^{[a], [g]}	–	726.6	672.0	692.7	843.4
NEVPT2 ^{[a], [g]}	–	995.3	1423.4	1230.9	1072.3
UHF ^[h]	611.0	–1624.7	–2805.0	–3030.1	–
UBLYP ^[h]	2037.1	1031.0	825.5	2261.8	–
UB3LYP ^[h]	1514.4	153.4	–284.1	839.6	–
UMP2 ^[h]	851.3	–1134.7	–2154.5	–1913.0	–
UMP3 ^[h]	852.1	–1101.5	–2109.1	–1857.2	–

All values are in cm^{-1} and the 6-311G* basis set was used unless stated otherwise.

[a] Difference of lowest energy singlet and triplet CAS(8,10) solutions.

[b] The particular multiplicity lowest energy state solutions have been expanded in the basis set of the singlet ground state CAS(8,8) solution.

[c] The particular multiplicity lowest energy state solutions have been expanded in the basis set of the nonet ground state CAS(8,10) solution.

[d] def2-TZVPP calculation.

[e] Restricted closed-shell calculation.

[f] Periodic pob-DZVP calculation.

[g] Taking the multiplicity S^2 factor $E_S = -(J/2)[S(S+1) - S_A(S_A+1) - S_B(S_B+1)]$ or $\Delta E_{M1-M5} = - (E_{M1} - E_{M5})/[S(S+1)]$, where S_A and S_B are partial spins on centers A and B, respectively.

[h] BS treatment according to eq. 2.

UMP2 and UMP3 ones) with the experimental J coupling value, while DFT overestimates the J values when using eq. 2. Another option for the J coupling estimate could be done via the ΔE_{M3-M1} difference using the results of the unrestricted single-determinant methods. Nevertheless, this seems troublesome due to the fact that both states (M1 and M3) suffer from BS and spin contamination, which affect the final value of energy difference and the correction is not straightforward.

Comparison of UHF/UDFT and CAS states

Compound (I). A notable feature to be mentioned here is the different character of the UHF BS singlet (spin up and spin down) and the CAS (closed-shell) wave functions. The singlet spin state in the UHF BS approach is a single-reference determinant with spin up and spin down on each of the copper centers, while the CAS singlet ground-state wave function has a closed-shell character (no spin density at all). The restricted open Hartree-Fock (ROHF) and CAS triplet wave functions have an identical single-determinant character which is furthermore confirmed by the Löwdin d-orbital populations and bond orders, see Table 4. Furthermore, as already mentioned above the open shell orbitals (with respect to their eigenvalues) lay deep in the orbital sea in the case of UHF calculations. Hence it is not straightforward to identify the magnetic orbitals in the UHF calculation while in the UB3LYP and UBLYP calculations

the frontier orbitals (HOMO and LUMO) can be associated with the open-shell (magnetic) orbitals. An extended discussion of open-shell (magnetic) orbitals of compound (I) is accounted for within the Supporting Information.

The CAS(18,10) active space of the M1 ground state is depicted in Figure 3a, the active orbitals ordering is due to the particular eigenvalues. Considering the shapes of the orbitals, one can see that the EBO^[19] is formally zero according to the balance in the bonding and antibonding character of the $\delta_{B2g}\delta_{B2g}^*\pi_{Eg}\pi_{Eg}\sigma_{A1g}\pi_{Eg}^*\pi_{Eg}^*\sigma_{A1g}^*\delta_{B1g}\delta_{B1g}^*$ active space. An extended discussion of open-shell (magnetic) orbitals of compound (I) is accounted for within the Supporting Information.

Compound (II). The M9 CAS state is confirmed to be a single-determinant wave function matching the ROHF results (see the following section). Similar as in the case of (I) the M9 ROHF eigenvalues are considerably lower than the CAS ones, despite the same total energy values. The spatial overlaps $\Sigma_j \langle i_{\alpha} j_{\beta} \rangle$ prove that the open shells of the UHF calculations are deeper in the frontier orbitals sea comparing to UB3LYP and especially to UBLYP orbitals. The UBLYP (as well as UB3LYP) open-shell orbitals are essentially the top eight occupied α -MOs (or lowest eight unoccupied β -MOs). Still, the UHF spin polarization of the closed shells in (II) is considerably lower than in (I). The M1 CAS multideterminant wavefunction has the largest contributions from the $\sigma_{A1g}\pi_{Eg}\pi_{Eg}\delta_{B2g}$ closed-shell determinant with a weight

Table 4. Löwdin (total and spin density) orbital populations of Cu₁ in (I) and WBOs of Cu₁ coordination polyhedron.

		M ³ UB3LYP	M ¹ UB3LYP	M ³ UBLYP	M ¹ UBLYP	M ³ ROB3LYP	M ¹ RB3LYP
Charge	s	0.478	0.528	0.503	0.578	0.529	0.498
	d _{z2}	1.968	1.967	1.947	1.947	1.968	1.960
	d _{xz}	1.987	1.987	1.982	1.982	1.987	1.984
	d _{yz}	1.986	1.985	1.980	1.980	1.986	1.983
	d _{x2-y2}	1.340	1.343	1.443	1.449	1.338	1.476
	d _{xy}	1.985	1.985	1.972	1.972	1.985	1.980
	Spin	s	-0.008	0.008	-0.006	0.004	0.000
d _{z2}		0.004	-0.005	0.004	-0.006	0.000	
d _{xz}		0.001	-0.001	0.001	-0.001	0.000	
d _{yz}		0.002	-0.002	0.002	-0.002	0.001	
d _{x2-y2}		0.700	-0.695	0.590	-0.561	0.706	
d _{xy}		0.004	-0.004	0.004	-0.004	0.003	
WBO		Cu ₂	0.078	0.080	0.099	0.123	0.078
	O ₁₋₄	0.259	0.259	0.270	0.269	0.258	0.260
	O _W	0.127	0.127	0.136	0.136	0.127	0.127
		M ³ UHF	M ¹ UHF	M ³ ROHF	M ¹ RHF	M ³ CAS	M ¹ CAS
Charge	s	0.393	0.348	0.348	0.376	0.348	0.348
	d _{z2}	1.996	1.996	1.996	1.992	1.996	1.996
	d _{xz}	1.996	1.996	1.996	1.994	1.996	1.996
	d _{yz}	1.995	1.995	1.995	1.993	1.995	1.995
	d _{x2-y2}	1.135	1.135	1.131	1.372	1.131	1.132
	d _{xy}	1.997	1.997	1.997	1.996	1.997	1.997
	Spin	s	-0.006	0.008	0.000		0.000
d _{z2}		0.003	-0.004	0.001		0.001	
d _{xz}		0.002	-0.002	0.001		0.001	
d _{yz}		0.002	-0.002	0.001		0.001	
d _{x2-y2}		0.919	-0.918	0.929		0.929	
d _{xy}		0.004	-0.004	0.004		0.004	
WBO		Cu ₂	0.052	0.041 ^[a]	0.040 ^[a]	0.479	0.040 ^[a]
	O ₁₋₄	0.212	0.212	0.211	0.231	0.211	0.211
	O _W	0.102	0.106	0.106	0.104	0.106	0.106

6-311G* basis set was used; M3 and M1 denote triplet and singlet state calculations, respectively.

[a] MultiWFN program has been used to yield WBO values below 0.05.

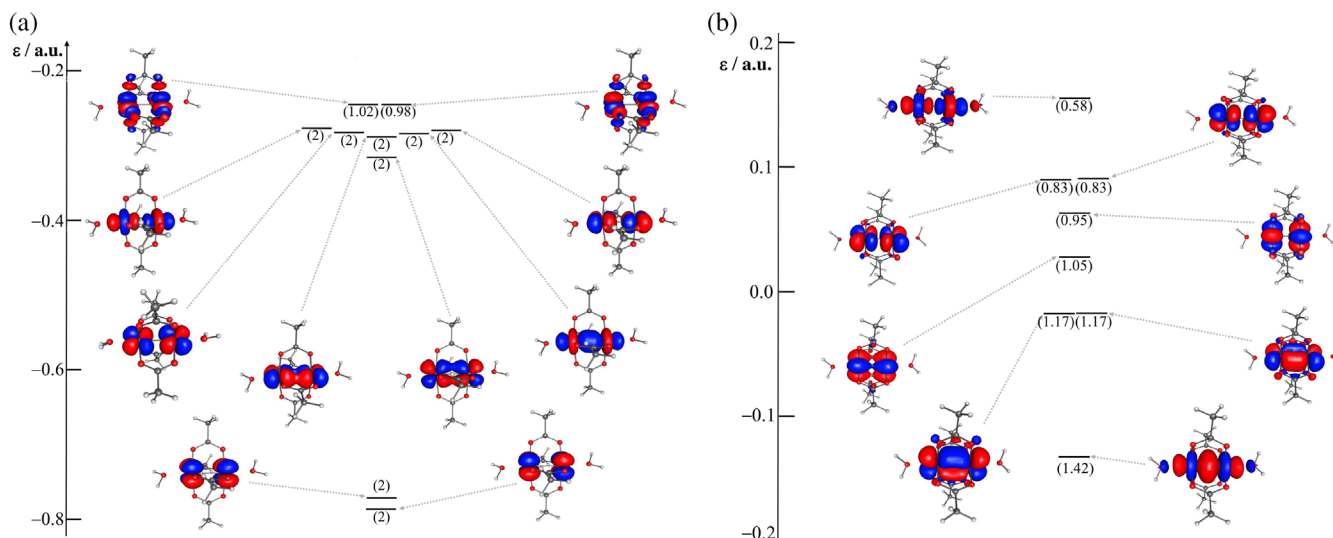


Figure 3. CAS active space orbitals of a) compound (I) and b) compound (II). [Color figure can be viewed at wileyonlinelibrary.com]

of 7.5%, and the M1 CAS determinants have a 40% closed-shell character (contain only empty or double occupied active orbitals). Still, the overall spin density is zero in the multi-determinant M1 case. (In the case of the dehydrated form of (II), the weights of $\sigma_{A1g}\pi_{Eg}\pi_{Eg}\delta_{B2g}$ and $\sigma_{A1g}\pi_{Eg}\pi_{Eg}\delta_{B2g}^*$ determinants are 26.4% and 14.2%, respectively [Cr—Cr distance of 1.966 Å].)

The CAS(8,8) active space orbitals ($\sigma_{A1g}\pi_{Eg}\pi_{Eg}\delta_{B2g}\delta_{B2g}^*\pi_{Eg}^*\pi_{Eg}^*\sigma_{A1g}^*$) of the M1 ground state are depicted in Figure 3b. Considering the bonding ($w_b = 1$) and antibonding ($w_a = -1$) interactions in the active space of (II) and weighting (w) the occupation numbers accordingly, one yields an EBO (formal) equal to 0.8 e as is suggested in Roos et al.^[19] with the formula $EBO = (n_b - n_a)/2$. Still, because of the strong bonding/nonbonding/antibonding character of d orbitals and no further hybridization of the d orbitals with s and p ones (and/or due to the presence of nodal surface [nonbonding contributions]), a considerable part of the charge density (approx. one half) is out of the bonding region for the σ_{A1g} and π_{Eg} interactions (see Fig. 3b), while the net contribution of δ_{B2g} orbitals is almost zero. Hence, we find it appropriate to scale the formal EBO by a factor of two to estimate the physical EBO to 0.4 e which is in reasonable agreement with the WBO for this M1 CAS calculation (0.303 e), see Table 5. Similarly in the dehydrated form of (II) with $d(\text{Cr—Cr}) = 1.966 \text{ \AA}$, we find a formal EBO^[19] of 1.86 e which leads to the physical EBO estimate of 0.93 e , while the WBO yields 1.12 e which is closer to the physical EBO estimate. When elongating the Cr—Cr bond length by 0.5 Å in the dehydrated form of (II), the formal EBO, physical EBO, and WBO values are 0.60, 0.30, and 0.19 e , respectively.

AO-based population analyses

Compound (I). The Löwdin atomic populations and the WBOs of (I) for CuI central atom are compiled in Table 4. The $d_{x^2-y^2}$

AO is identified as the open shell in the triplet state, considering the total d AO populations (having a value below 1.5 in each case) as well as spin populations (being above 0.5). Naturally, these values are the largest for the ab initio methods (overestimated spin localization on the central metal atoms), followed by the hybrid (UB3LYP) and the pure (UBLYP) DFT functionals. Herich et al.^[6] and Bertolotti et al.^[28] report d-populations of similar magnitude for the SCXD-derived multipole model charge density. The WBOs show that the Cu—O_w dative bonds are by about a factor of half weaker than Cu—O₁₋₄ ones, see Table 4. Cu—Cu WBOs are low in the case of the unrestricted calculations, where these values hardly exceed 0.1 e (only in the case of the BS M1 UBLYP is this value 0.123 e , where Shee et al.^[9] obtained a value of 0.30 for the BP86 functional). The larger WBO values at the DFT levels of theory seem to correlate with the spin delocalization for (I). Furthermore, one can immediately see that the direct M—M interaction (WBO) are proportional to $\Delta E_{U,M3-M1}$ (and/or energy stabilization of the low spin state). Hence, the spin delocalization on ligands does not lead to a ligand bridge mediated magnetic interaction but rather stimulates the direct M—M exchange. Still, the low CAS and BS WBO values suggest very weak bonding interactions between the copper atoms in (I).

The restricted singlet calculations provide the largest Cu—Cu bond orders, nevertheless these are accounted for just for completeness and cannot be made justified with respect to their energetics (see Table 2). The Löwdin atomic charges and spin populations agree reasonably well with the QTAIM results (see the following section and compare Table 6 and Supporting Information Table S3).

Compound (II). In the case of (II), the AO d populations on Cr identify the $d_{x^2-y^2}$ AO as the empty d-shell irrespective of multiplicity, see Table 5. The d populations reported in Herich et al.^[6] agree reasonably well with Löwdin orbital populations in Table 5. CAS AO spin populations of different multiplicities are

Table 5. Löwdin (total and spin density) orbital populations of Cr₁ in (II) and WBOs of Cr₁ coordination polyhedron.

		M ⁹ CAS	M ⁷ CAS	M ⁵ CAS	M ³ CAS	M ¹ CAS	M ⁹ ROHF	M ¹ RHF
Charge	s	6.309	6.318	6.322	6.325	6.326	6.309	6.312
	d _{z²}	1.050	1.042	1.038	1.037	1.036	1.050	0.688
	d _{xz}	1.009	1.009	1.009	1.008	1.008	1.009	1.346
	d _{yz}	1.008	1.007	1.007	1.007	1.006	1.008	1.027
	d _{x²-y²}	0.303	0.304	0.304	0.305	0.305	0.303	0.334
	d _{xy}	1.026	1.026	1.026	1.026	1.027	1.026	1.017
Spin	s	0.023	0.015	0.009	0.004	0.000	0.023	
	d _{z²}	0.940	0.543	0.310	0.143	0.000	0.940	
	d _{xz}	0.983	0.794	0.542	0.272	0.000	0.983	
	d _{yz}	0.984	0.795	0.543	0.272	0.000	0.984	
	d _{x²-y²}	0.001	0.001	0.001	0.000	0.000	0.001	
	d _{xy}	0.979	0.788	0.553	0.288	0.000	0.979	
WBO	Cr ₂	0.085	0.132	0.200	0.258	0.303	0.085	0.242
	O ₁₋₄	0.311	0.313	0.314	0.314	0.315	0.311	0.330
	Ow	0.128	0.125	0.124	0.123	0.123	0.128	0.156
	B3LYP	M ⁹ U	M ⁷ U	M ⁵ U	M ³ U	M ¹ U	M ⁹ RO	M ⁹ R
Charge	s	6.368	6.417	6.402	6.398	6.394	6.368	6.397
	d _{z²}	1.021	0.989	0.995	1.006	1.017	1.023	0.965
	d _{xz}	1.013	1.014	1.012	1.010	1.010	1.014	1.072
	d _{yz}	1.010	1.011	1.010	1.006	1.007	1.011	0.969
	d _{x²-y²}	0.437	0.441	0.443	0.444	0.443	0.431	0.469
	d _{xy}	1.021	1.023	1.024	1.024	1.020	1.022	1.048
Spin	s	0.052	0.008 (0.000)	0.021 (-0.011)	0.023 (-0.020)	0.026 (-0.026)	0.037	
	Cr ₁	d _{z²}	0.876	0.161 (-0.107)	0.513 (-0.432)	0.582 (-0.566)	0.644 (-0.644)	0.876
	(Cr ₂)	d _{xz}	0.964	0.965 (0.964)	0.937 (0.041)	0.919 (-0.902)	0.926 (-0.926)	0.964
	d _{yz}	0.964	0.966 (0.965)	0.937 (0.018)	0.929 (-0.536)	0.927 (-0.927)	0.965	
	d _{x²-y²}	0.054	0.045 (0.039)	0.051 (0.000)	0.053 (-0.034)	0.054 (-0.054)	0.001	
	d _{xy}	0.942	0.941 (0.940)	0.942 (0.875)	0.940 (0.531)	0.926 (-0.926)	0.944	
WBO	Cr ₂	0.114	0.838	0.698	0.664	0.584	0.114	1.764
	O ₁₋₄	0.373	0.390	0.385	0.384	0.384	0.373	0.429
	Ow	0.157	0.141	0.143	0.143	0.144	0.157	0.169

6-311G* basis set was used, labels M⁹, M⁷, M⁵, M³, M¹ represent the spin state and U, RO, and R denote the single-determinant unrestricted, restricted open and restricted methods, respectively. The Cr₂ spin AO populations of the BS results are presented in parenthesis.

closely related to the total S^2 and S_z spin projections (and/or spin populations on Cr). The CAS d_{xy}, d_{xz}, and d_{yz} AO spin populations of a particular multiplicity (M³—M⁹) are very similar which has to be correlated with the degeneracy

(eigenvalues) of these orbitals in the formally D_{4h} symmetry (see Fig. 3b), while the d_{z²} AO spin population is lower (having the lowest eigenvalue, see Fig. 3b). In the case of the UB3LYP, the BS singlet closely reflects a complete spin flip on one of the

Table 6. QTAIM charge (q) and spin densities at Cu, Cr, and O atoms of the experimental (X-ray) structure of (I) and (II).

(I)	q(Cu)	spin(Cu)	q(O ₁₋₄)	q(O _w)
UBLYP	1.13 ^{M1} , 1.09 ^{M3}	0.58 ^{M1} , 0.59 ^{M3}	-1.07 ^{M1} , -1.05 ^{M3}	-0.91 ^{M1} , -1.00 ^{M3}
UB3LYP	1.23 ^{M1} , 1.24 ^{M3}	0.71 ^{M1} , 0.71 ^{M3}	-1.15 ^{M1} , -1.15 ^{M3}	-0.95 ^{M1} , -0.95 ^{M3}
UB3LYP ^[a]	1.28 ^{M1} , 1.28 ^{M3}	0.70 ^{M1} , 0.70 ^{M3}	-1.11 ^{M1} , -1.12 ^{M3}	-1.32 ^{M1} , -1.32 ^{M3}
UHF	1.53 ^{M1} , 1.53 ^{M3}	0.92 ^{M1} , 0.92 ^{M3}	-1.38 ^{M1} , -1.38 ^{M3}	-1.06 ^{M1} , -1.06 ^{M3}
UMP2	1.37 ^{M1} , 1.37 ^{M3}	0.87 ^{M1} , 0.86 ^{M3}	-1.20 ^{M1} , -1.20 ^{M3}	-1.00 ^{M1} , -1.00 ^{M3}
CAS	1.56 ^{M1} , 1.56 ^{M3}	0.93 ^{M3}	-1.39 ^{M1} , -1.39 ^{M3}	-1.06 ^{M1} , -1.06 ^{M3}
B3LYP ^[b]	1.20		-1.15	-0.91
X-ray ^[b,c]	0.41		-0.96	-1.17
X-ray ^[d]	1.49		-1.02	-1.23
(II)	q(Cr)	spin(Cr)	q(O ₁₋₄)	q(O _w)
UBLYP	1.29 ^{M1} , 1.38 ^{M9}	2.76 ^{M1} , 3.64 ^{M9}	-1.09 ^{M1} , -1.11 ^{M9}	-1.07 ^{M1} , -0.97 ^{M9}
UB3LYP	1.40 ^{M1} , 1.42 ^{M9}	3.48 ^{M1} , 3.75 ^{M9}	-1.19 ^{M1} , -1.18 ^{M9}	-1.13 ^{M1} , -0.99 ^{M9}
UB3LYP ^[a]	1.40 ^{M1} , 1.42 ^{M9}	3.57 ^{M1} , 3.95 ^{M9}	-1.16 ^{M1} , -1.17 ^{M9}	-1.35 ^{M1} , -1.35 ^{M9}
UHF	1.60 ^{M1} , 1.61 ^{M9}	3.70 ^{M1} , 3.85 ^{M9}	-1.39 ^{M1} , -1.39 ^{M9}	-1.08 ^{M1} , -1.08 ^{M9}
CAS	1.61 ^{M1} , 1.62 ^{M9}	3.79 ^{M9}	-1.40 ^{M1} , -1.40 ^{M9}	-1.08 ^{M1} , -1.08 ^{M9}
X-ray ^[d]	1.55		-1.10	-1.30

Presented O₁₋₄ charges are average values of four oxygens of the acetate ligands. Basis set used is 6-311G* unless stated otherwise. BS spin density at the other Cu/Cr atom has an opposite sign in the case of M¹.

[a] Calculations carried out in CRYSTAL17 using pob-DZVP(without f) basis set.

[b] Calculated values taken from Bertolotti et al.^[28]

[c] Experimental multipole refinement values taken from Bertolotti et al.^[28]

[d] Experimental values taken from Herich et al.^[6]

Cr atoms as already seen in the case of **(I)** (being the energetically preferred state). The obtained BS UB3LYP/6-311G* ($\langle S^2 \rangle$) expectation values are 3.41, 4.30, 7.24, 12.02 for M1, M3, M5 and M7 multiplicities, respectively, see Supporting Information Table S1. These ($\langle S^2 \rangle$) expectation values are very similar at the UHF and UBLYP levels of theory, see Supporting Information Table S1. The WBOs of **(II)** are larger for M1 in comparison with M9 calculations, when considering CAS and UB3LYP results in Table 5. The overall CAS M1 WBO between Cr–Cr atoms is 0.303 which is nearly half smaller when comparing to the UB3LYP one (0.584), but it is still about five times larger than in the case of **(I)**. (Note that in the case of UBLYP method is the Cr–Cr WBO 1.036 in value, not shown in Table 5, which can be further justified with the too short optimized Cr–Cr bond distances when using non-hybrid functionals.) As already discussed for **(I)**, the strength of the M–M interaction correlates closely with the $\Delta E_{U,M9-M1}$ value in **(II)** pointing toward the direct magnetic coupling between the metal spin centers. The Löwdin total charges and spin populations of **(II)** (see Supporting Information Table S4) agree qualitatively well with the QTAIM analysis (see the following section).

QTAIM analysis and electron density topology

QTAIM analysis of BCPs and DIs are a useful tool to obtain additional information on the nature and character of chemical bonds. According to Bader's theory, the BCP is a saddle point of electron density between the two atoms.^[73] The DI is a measure of the number of electrons that are shared (or exchanged) between the two atoms being a synonym for the bond order.^[89] Charge and spin densities at Cu and Cr are presented in Table 6. BCP charge densities ρ_{BCP} , Laplacians L_{BCP} and DIs of M–M and M–O bonds in the studied systems are presented in Tables 7 and 8.

Compound (I). The agreement between the calculated CAS or UHF and experimentally obtained charge^[6] on Cu is very good (1.56 e vs. 1.49 e), see Table 6. At the DFT level of theory, the positive charge on the Cu atom is lower when comparing to CAS, UHF method and the X-ray experiment reported by Herich et al.^[6] while the Cu charge derived experimentally in Bertolotti et al.^[28] is underestimated by a factor of three. The spin delocalization at the DFT levels of theory is immediately seen from the QTAIM spin density on Cu, which affects also the total charge of coppers. Oxygens of acetate ligands (O_{1-4}) have the calculated charges more negative than the ones of water molecules (O_W) while in the experiment^[6,28] is the charge of O_W larger (more negative) than of O_{1-4} , see Table 6. The situation becomes improved with respect to the experimentally determined charges of oxygens in the case of periodic calculations carried out in CRYSTAL17. These calculations provide slightly more negative charges for O_W oxygens what is in better agreement with previously published experimental data.^[6,28] This can be related to the importance of intermolecular hydrogen bond interactions of the water molecule, which allow for a larger charge on the O_W atom. Nevertheless, we should mention that in the multipole model expansion of the experimental SCXD

refined charge density, the oxygen atoms were treated with a single set of radial contraction parameters.

Our calculated UB3LYP BCP parameters of **(I)** are in a qualitative agreement with the results published by Bertolotti et al.^[28] and Herich et al.,^[6] see Table 7. This agreement is generally better in the case of Cu–O bonds comparing to the Cu–Cu one. The closest agreement with X-ray experiment^[6] for the Cu–Cu ρ_{BCP} value is found for the CAS (and/or UHF) method, albeit the calculated values are still overestimated by a factor of two. Hence, the particular DIs (or WBOs) can be considered slightly overestimated with respect to the experiment. Nevertheless, the insufficient radial flexibility of multipole model charge density has to be critically mentioned, leading to an underestimated M–M interaction.^[90] The UB3LYP ρ_{BCP} values are larger than the UHF, UMP2, and CAS ones especially in the Cu–Cu bond case, which is even more pronounced for the pure UBLYP functional. Still, these UDFT values are well in line with trends in DIs, WBOs, $\Delta E_{U,M3-M1}$ and the spin delocalization in **(I)** for the different methods. Moreover, it is fair to stress that the UMP2 values are shifted toward the UB3LYP ones, when compared to UHF level of theory.* One can also see that there is basically no qualitative difference between the values calculated for singlet and triplet states (compare M1 and M3 values). Also notice from Table 7, that all the Laplacian values ($L_{\rho_{BCP}}$) reported by Shee et al.^[91] are completely different than the rest of Table 7 as pointed out in Herich et al.^[6] (including a different/wrong sign). This error was probably caused by the incorrect unit conversion using a bohr⁻³ to Å⁻³ instead of the correct bohr⁻⁵ to Å⁻⁵ one. According to Table 7, the Cu– O_W bond is found weaker by a factor of two when compared to Cu– O_{1-4} ones, considering ρ_{BCP} and DI values. This is well in line with WBOs and matches the conclusion of Herich et al.^[6] about the electrostatic character of the Cu– O_W interaction in **(I)**.

Compound (II). In the case of **(II)**, DFT level of theory underestimates the positive charge on the Cr atom as is the case of **(I)**, see Table 6. The agreement between the calculated CAS and experimentally derived multipole model charges at Cr atoms is again very good (1.61/1.60 e vs. 1.55 e, respectively). Furthermore, the general features in the oxygen charges of **(II)** are also matching closely with **(I)**, vide supra.

BCP characteristics of Cr–Cr and Cr–O bonds in **(II)** for M1 and M9 multiplicities at CAS and the single-reference UHF, UBLYP, and UB3LYP levels of theory are compiled in Table 8. The complete CAS, UBLYP, and UB3LYP data (i.e., M = 1, 3, 5, 7, 9) can be found in Supporting Information Table S6. As can be seen from Table 8 and Supporting Information Table S6, the CAS values have well defined trends, that is, Cr–Cr BCP charge densities (ρ_{BCP}) as well as DI values are decreasing with the increasing multiplicity of the system. The UHF BCP parameters as well as DI values correspond well with CAS ones.[†] This is in agreement with the relative stability of **(II)** with respect to the

In the case of Cu_2^{2+} and Cu_2^{4+} UHF/6-311+G DI values are 0.131 and 0.060, respectively (Cu–Cu bond length is 2.6108 Å).

†In the case of Cr_2^{2+} and Cr_2^{4+} UHF/6-311+G* DI values are 1.187 and 0.412, respectively (Cr–Cr bond length is 2.349 Å).

Table 7. QAIM BCP characteristics, that is, charge density ρ_{BCP} , Laplacian L_{BCP} , and DI of the X-ray structure of (I), where subscripts W and 1–4 follows the atoms labeling in Figure 1.

BCP	ρ_{BCP} ($e \text{ \AA}^{-3}$)	L_{BCP} ($e \text{ \AA}^{-5}$)	DI (-)
UBLYP			
Cu–Cu	0.185 ^{M1} , 0.185 ^{M3}	1.979 ^{M1} , 1.979 ^{M3}	0.154 ^{M1} , 0.130 ^{M3}
Cu–O _W	0.364 ^{M1} , 0.364 ^{M3}	5.700 ^{M1} , 5.698 ^{M3}	0.245 ^{M1} , 0.244 ^{M3}
Cu–O _{1–4}	0.568 ^{M1} , 0.567 ^{M3}	9.873 ^{M1} , 9.899 ^{M3}	0.439 ^{M1} , 0.445 ^{M3}
UB3LYP			
Cu–Cu	0.167 ^{M1} , 0.167 ^{M3}	2.014 ^{M1} , 2.015 ^{M3}	0.103 ^{M1} , 0.102 ^{M3}
Cu–O _W	0.356 ^{M1} , 0.356 ^{M3}	5.850 ^{M1} , 5.848 ^{M3}	0.226 ^{M1} , 0.226 ^{M3}
Cu–O _{1–4}	0.559 ^{M1} , 0.559 ^{M3}	10.214 ^{M1} , 10.225 ^{M3}	0.416 ^{M1} , 0.417 ^{M3}
UB3LYP ^[a]			
Cu–Cu	0.216 ^{M1} , 0.216 ^{M3}	0.578 ^{M1} , 0.578 ^{M3}	
Cu–O _W	0.344 ^{M1} , 0.344 ^{M3}	6.868 ^{M1} , 6.868 ^{M3}	
Cu–O _{1–4}	0.521 ^{M1} , 0.521 ^{M3}	12.013 ^{M1} , 12.019 ^{M3}	
UHF			
Cu–Cu	0.121 ^{M1} , 0.120 ^{M3}	1.995 ^{M1} , 1.996 ^{M3}	0.050 ^{M1} , 0.050 ^{M3}
Cu–O _W	0.328 ^{M1} , 0.328 ^{M3}	6.369 ^{M1} , 6.369 ^{M3}	0.182 ^{M1} , 0.182 ^{M3}
Cu–O _{1–4}	0.546 ^{M1} , 0.545 ^{M3}	13.222 ^{M1} , 13.224 ^{M3}	0.327 ^{M1} , 0.327 ^{M3}
UMP2			
Cu–Cu	0.153 ^{M1} , 0.153 ^{M3}	2.075 ^{M1} , 2.076 ^{M3}	0.050 ^{M1} , 0.050 ^{M3}
Cu–O _W	0.347 ^{M1} , 0.347 ^{M3}	5.962 ^{M1} , 5.962 ^{M3}	0.196 ^{M1} , 0.196 ^{M3}
Cu–O _{1–4}	0.579 ^{M1} , 0.578 ^{M3}	11.705 ^{M1} , 11.710 ^{M3}	0.364 ^{M1} , 0.364 ^{M3}
CAS			
Cu–Cu	0.113 ^{M1} , 0.113 ^{M3}	1.930 ^{M1} , 1.930 ^{M3}	0.046 ^{M1} , 0.046 ^{M3}
Cu–O _W	0.323 ^{M1} , 0.323 ^{M3}	6.534 ^{M1} , 6.534 ^{M3}	0.178 ^{M1} , 0.178 ^{M3}
Cu–O _{1–4}	0.532 ^{M1} , 0.532 ^{M3}	13.200 ^{M1} , 13.202 ^{M3}	0.285 ^{M1} , 0.318 ^{M3}
Relevant published data			
Cu–Cu	0.199 ^[b] , 0.202 ^[c] , 0.057 ^[d]	1.58 ^[b] , –0.24 ^[c] , 1.648 ^[d]	0.129 ^[b]
Cu–O _W	0.349 ^[b] , 0.202 ^[c] , 0.295 ^[d]	6.08 ^[b] , –0.96 ^[c] , 7.026 ^[d]	0.248 ^[b]
Cu–O _{1–4}	0.566 ^[b] , 0.472 ^[c] , 0.440 ^[d]	11.56 ^[b] , –2.89 ^[c] , 11.876 ^[d]	0.373 ^[b]

In the case of Cu–O bonds average values are presented, complete set of data is provided in Supporting Information Table S5. Basis set used is 6-311G* unless stated otherwise. Comparison to relevant published data is also given.

[a] Calculations carried out in CRYSTAL17 using pob-DZVP(without f) basis set.

[b] Calculated values taken from Bertolotti et al.^[28]

[c] Calculated values taken from Shee et al.^[9]

[d] Experimental values taken from Herich et al.^[6]

different spin states (see Table 3), pointing out that the strongest Cr–Cr bond is present in the energetically preferred singlet spin state (M1). Cr–O BCP parameters as well as QAIM charges at oxygens are not affected by the changes of spin states in (II), see Tables 6 and 8. One can see that the DFT BCP parameters of Cr–O bonds are in a qualitative agreement with the CAS ones (see Table 8 and Supporting Information Table S6). The Cr–Cr interaction is found weaker than the Cr–O_{1–4} ones at the UHF and CAS levels of theory, while the opposite is true for the DFT results. The UB3LYP and/or UBLYP M1 DIs of Cr–Cr bond are approximately two and/or four times larger when comparing to the CAS M1 value, respectively (a very similar situation is found for the WBO values, see Table 5). The overestimated UBLYP DI value corresponds to the shorter Cr–Cr distance of the UBLYP optimized geometry when compared to UB3LYP (and/or X-ray structure). The strength of the Cr–Cr interaction at a given level of theory is found proportional to J coupling. Although, the comparison of CAS and DFT QAIM results correlates less with the found J coupling. This can be made related to the multideterminant character of the wave function and the one particle reduced density matrix approximation used in the evaluation of CAS DIs. All the theoretically determined Cr–Cr ρ_{BCP} values are overestimated with respect to the experimental multipole refinement results reported in Herich et al.^[6] Hence, it

appears reasonable to argue that the determined theoretical DIs and/or WBOs are also overestimated, when assuming proportionality of DIs with ρ_{BCP} values, as already seen for (I). Nevertheless, the insufficient radial flexibility of multipole model charge density has to be mentioned again, leading to an underestimated M–M interaction also in the case of (II).^[90] One can also notice from the comparison of ρ_{BCP} and DI values that the Cr–Cr bond is significantly stronger than the Cu–Cu one, cf. Tables 7 and 8. This is further confirmed by the ELF analysis, see the following section.

Electron localization function

Herein, we make use of the ELF which is able to identify pictorially bonding interactions upon the behavior of electron pair density.^[78] As introduced by Becke and Edgecombe, ELF is a measure of the probability to find an electron in the neighborhood of another electron, that is, being a measure of Pauli repulsion.^[77] In the case of BS M1 UB3LYP results of 3D ELF visualization, one cannot identify any interactions in the Cu–Cu region in (I), see Figure 4a, while a direct Cr–Cr bond interaction can be clearly identified for (II), see Figure 4b. It has to be mentioned that the isovalue of 0.4 necessary to visualize the Cr–Cr interaction in (II) of Figure 4 is smaller than the

Table 8. QTAIM BCP characteristics, that is, charge density ρ_{BCP} , Laplacian L_{BCP} , and DI of the X-ray structure of (II), with different multiplicities (M1, M9).

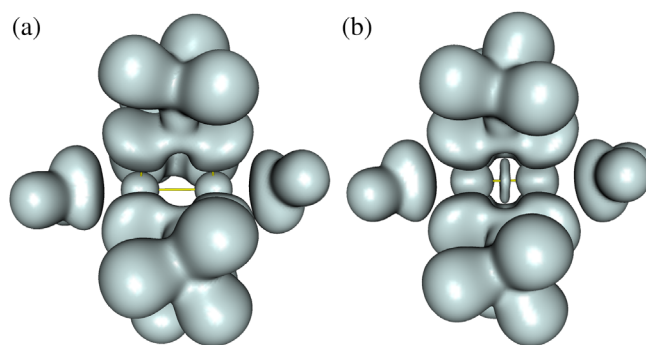
BCP	ρ_{BCP} (e \AA^{-3})	L_{BCP} (e \AA^{-5})	DI (-)
UBLYP			
Cr–Cr	0.543 ^{M1} , 0.362 ^{M9}	1.450 ^{M1} , 3.480 ^{M9}	1.054 ^{M1} , 0.280 ^{M9}
Cr–O _W	0.298 ^{M1} , 0.307 ^{M9}	5.247 ^{M1} , 5.039 ^{M9}	0.225 ^{M1} , 0.278 ^{M9}
Cr–O _{1–4}	0.523 ^{M1} , 0.527 ^{M9}	10.131 ^{M1} , 10.118 ^{M9}	0.457 ^{M1} , 0.447 ^{M9}
UB3LYP			
Cr–Cr	0.513 ^{M1} , 0.347 ^{M9}	1.730 ^{M1} , 3.960 ^{M9}	0.665 ^{M1} , 0.259 ^{M9}
Cr–O _W	0.292 ^{M1} , 0.301 ^{M9}	5.394 ^{M1} , 5.293 ^{M9}	0.211 ^{M1} , 0.231 ^{M9}
Cr–O _{1–4}	0.513 ^{M1} , 0.516 ^{M9}	10.538 ^{M1} , 10.562 ^{M9}	0.414 ^{M1} , 0.406 ^{M9}
UB3LYP^[a]			
Cr–Cr	0.492 ^{M1} , 0.331 ^{M9}	2.506 ^{M1} , 4.916 ^{M9}	
Cr–O _W	0.297 ^{M1} , 0.304 ^{M9}	5.446 ^{M1} , 5.543 ^{M9}	
Cr–O _{1–4}	0.488 ^{M1} , 0.491 ^{M9}	11.128 ^{M1} , 11.110 ^{M9}	
UHF			
Cr–Cr	0.387 ^{M1} , 0.301 ^{M9}	3.630 ^{M1} , 4.822 ^{M9}	0.276 ^{M1} , 0.183 ^{M9}
Cr–O _W	0.275 ^{M1} , 0.278 ^{M9}	5.891 ^{M1} , 5.875 ^{M9}	0.169 ^{M1} , 0.171 ^{M9}
Cr–O _{1–4}	0.477 ^{M1} , 0.479 ^{M9}	12.023 ^{M1} , 12.022 ^{M9}	0.315 ^{M1} , 0.316 ^{M9}
CAS			
Cr–Cr	0.396 ^{M1} , 0.282 ^{M9}	3.830 ^{M1} , 5.285 ^{M9}	0.268 ^{M1} , 0.170 ^{M9}
Cr–O _W	0.274 ^{M1} , 0.276 ^{M9}	5.795 ^{M1} , 5.842 ^{M9}	0.162 ^{M1} , 0.173 ^{M9}
Cr–O _{1–4}	0.475 ^{M1} , 0.477 ^{M9}	11.637 ^{M1} , 11.659 ^{M9}	0.305 ^{M1} , 0.310 ^{M9}
X-ray^[b]			
Cr–Cr	0.167	4.944	
Cr–O _W	0.252	5.690	
Cr–O _{1–4}	0.424	11.989	

Subscripts W and 1–4 follows the atoms labeling in Figure 1. Basis set used is 6-311G* unless stated otherwise. In the case of Cr–O bonds average values are presented.

[a] Calculations carried out in CRYSTAL17 using pob-DZVP(without f) basis set.

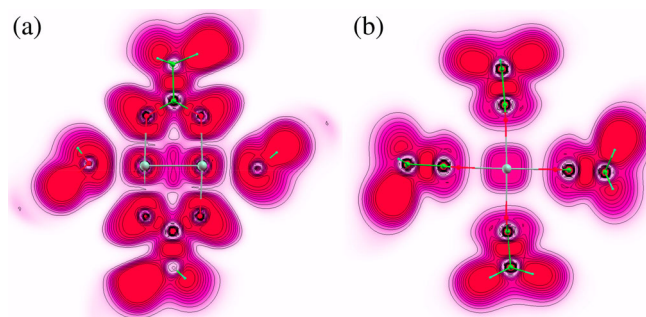
[b] Experimental values taken from Herich et al.^[6]

homogenous gas value (0.5). In the case of (I), the Cu–Cu interactions cannot be identified in the ELF plots neither for 0.2 nor 0.1 isovalue (not shown). On the other hand, the Cr–Cr regions of (II) become joined within a single surface (no mid-bonding ELF region can be obtained) in the BS M1 UHF (or M1 CAS) 3D ELF plot for isovalue 0.25 (or 0.15), see Supporting Information Figure S3. For comparison, Lepetit et al.^[3] have used the isovalue of 0.45 for the visualization of the quadruple Mo–Mo bond with DI = 2.93 at a bond distance of 2.092 \AA ^[91] in the bimetallic [Mo₂(formamidinate)₄] complex. The aforementioned Cr–Cr interaction is further manifested in the 2D ELF plots of (II) with clearly visible ELF bonding regions between the Cr atoms, see Figure 5. According to Jerabek et al.,^[10] in the dehydrated form of (I) a much smaller ELF isovalue needs to be taken into account to make the Cu–Cu interaction (very hardly) discernible in the 2D plot.

**Figure 4.** B3LYP/6-311G* 3D ELF plot of a) compound (I), b) compound (II), drawn at 0.4 isovalue. [Color figure can be viewed at wileyonlinelibrary.com]

Conclusions

The geometry of (I) can be well determined using both the DFT methods and the single-reference dynamic electron correlation methods (MP2, MP3, CCSD), except the orientation of the water ligands, when compared to the X-ray structure.^[6] The CAS/NEVPT2 singlet or BS singlet is identified as the energetically preferred spin state. However, the MP2 approach (including its double hybrid DFT clones) yields a wrong closed-shell reference ground state what can be corrected for by means of using the MP3 or CCSD levels of theory. The electronic structure study (QTAIM and ELF analysis) confirms only weak bonding interactions (below 0.1 e) between the two distant Cu centers. The metal–metal interactions are slightly overestimated in comparison with QTAIM analysis of charge density derived upon the X-ray experiment of Herich et al.^[6] ΔE_{M3-M1} and/or J coupling constant are being underestimated to 100 cm^{-1} for ab initio methods when not treating the spin delocalization with respect to the J evaluation in the BS single-determinant ab initio treatments and or CAS/NEVPT2 active space. These values are underestimated by at least a factor of two when compared to experimental or DFT results for a hybrid functional (in this case B3LYP). Still, if one accounts for the BS energy correction, the DFT J values are overestimated by a factor of two. Essentially, DFT leads to a larger spin delocalization to acetate ligand oxygens and stronger M–M interactions of (I) when

**Figure 5.** B3LYP/6-311G* 2D ELF plots of compound (II) in the Cr–Cr–O₁ plane (a) and the plane crossing the Cr–Cr mid-bond perpendicular to the C_{4v} symmetry axis with respect to the acetyl ligands b), drawn with 9 isovalues in the 0 (white) to 0.8 (red) range. [Color figure can be viewed at wileyonlinelibrary.com]

compared to ab initio results what closely correlates with the ΔE_{M3-M1} values. Hence, the spin delocalization to ligands does not lead to a ligand bridge mediated magnetic interaction but rather stimulates the direct M–M exchange. This shows on the fact that the state energetics of (I) presents a challenge for advanced ab initio methods benchmarking (including the particular electronic structure with respect to the spin delocalization).^[92–94] Albeit, a critical reevaluation of the experimentally determined J value could possibly play a crucial twist of the conclusion about the theoretical methods performance.

In the case of (II), the geometry optimization needs to account for static and dynamic electron correlation with NEVPT2 PES scan performing very well. The Cr–Cr double potential well character is found in (II) and its dehydrated form, as shown previously in Andersson et al.,^[30] with the double potential well-being much more pronounced in the dehydrated form. In the case of (II), the spin density is preferably localized at the Cr atoms and hence NEVPT2 performs very well for the J coupling evaluation when comparing to experiment and previous works.^[30,33] As already mentioned for (I), the amount of spin delocalization affects the direct M–M interaction strengths at different levels of theory, which also correlates with the ΔE_{M9-M1} and/or J coupling of (II). The electronic structure study uncovers a moderate physical bond order of around 0.3–0.4 e for the Cr–Cr bond when taking into consideration the WBOs and DIs, while the CAS (formal) EBO is found around 0.8 e. This value can be scaled down by a factor of two to take into account the nonbonding character (including the nodal behavior) of the d orbitals (especially of d_{z^2} , d_{xz} , and d_{yz} ones) which contribute the most to the difference between the bonding and antibonding interactions in the (formal) EBO, reflecting thus the obtained bond orders. When compared to the multipole model charge density derived from the SCXD experiment, the Cr–Cr BCP characteristics are overestimated with the best agreement found for the M1 CAS level of theory. In general, both studied systems appear as good candidates for testing the flexibility of charge density models derived upon least squares fit to structure factors from SCXD experiments.^[95–99]

Acknowledgments

Miroslav Kohout (MPI CPFS, Dresden, Germany) is greatly acknowledged for his valuable critical comments on the terminology used and the approximate evaluation of DIs via natural orbitals. Financial support was obtained from Slovak Grant Agencies APVV (contract Nos. APVV-15-0053 and APVV-15-0079) and VEGA (contracts No. 1/0598/16, 1/0466/18 and 1/0718/19). We are also grateful to the HPC center at the Slovak University of Technology in Bratislava, which is a part of the Slovak Infrastructure of High Performance Computing (SIVVP project, ITMS code 26230120002, funded by the European Region Development Funds) for the computational time and resources made available. We thank the Ministry of Education, Science, Research and Sport of the Slovak Republic for funding within the scheme “Excellent research teams”. To all financing sources the authors are greatly indebted.

Conflict of Interest

The authors declare that they have no conflict of interest.

Keywords: electronic structure · metal–metal interaction · paddle-wheel · population analysis · QAIM analysis

How to cite this article: M. Malček, B. Vénosová, I. Puškárová, J. Kožíšek, M. Gall, L. Bučinský. *J. Comput. Chem.* **2020**, *41*, 698–714. DOI: 10.1002/jcc.26121

 Additional Supporting Information may be found in the online version of this article.

- [1] L. F. Dahl, E. Ishishi, R. E. Rundle, *J. Chem. Phys.* **1957**, *26*, 1750.
- [2] R. H. D. Lyngdoh, H. F. Schaefer, R. B. King, *Chem. Rev.* **2018**, *118*, 11626.
- [3] C. Lepetit, P. Fau, K. Fajerweg, M. L. Kahn, B. Silvi, *Coord. Chem. Rev.* **2017**, *345*, 150.
- [4] F. A. Cotton, E. A. Hillard, C. A. Murillo, H. Zhou, *J. Am. Chem. Soc.* **2000**, *122*, 416.
- [5] A. C. Tzipis, *Coord. Chem. Rev.* **2017**, *345*, 229.
- [6] P. Herich, L. Bučinský, M. Breza, M. Gall, M. Fronc, V. Petříček, J. Kožíšek, *Acta Crystallogr. Sect. B Struct. Sci. Cryst. Eng. Mater.* **2018**, *74*, 681.
- [7] J. Kožíšek, N. K. Hansen, H. Fuess, *Acta Crystallogr. Sect. B Struct. Sci.* **2002**, *58*, 463.
- [8] R. Scatena, Y. T. Guntern, P. Macchi, *J. Am. Chem. Soc.* **2019**, *141*, 9382.
- [9] N. K. Shee, R. Verma, D. Kumar, D. Datta, *Comput. Theor. Chem.* **2015**, *1061*, 1.
- [10] P. Jerabek, B. Von Der Esch, H. Schmidbaur, P. Schwerdtfeger, *Inorg. Chem.* **2017**, *56*, 14624.
- [11] M. Kyuzou, W. Mori, J. Tanaka, *Inorganica Chim. Acta* **2010**, *363*, 930.
- [12] B. N. Figgis, R. L. Martin, *J. Chem. Soc.* **1956**, 3837. <https://doi.org/10.1039/JR9560003837>
- [13] D. M. L. Goodgame, N. J. Hill, D. F. Marsham, A. C. Skapski, M. L. Smart, P. G. H. Troughton, *Chem. Commun.* **1969**, 448, 629.
- [14] K. A. Peterson, C. Puzzarini, *Theor. Chem. Acc.* **2005**, *114*, 283.
- [15] E. Pahl, D. Figgen, A. Borschevsky, K. A. Peterson, P. Schwerdtfeger, *Theor. Chem. Acc.* **2011**, *129*, 651.
- [16] S. A. Sadjadi, C. F. Matta, I. Hamilton, *Can. J. Chem.* **2013**, *91*, 583.
- [17] B. O. Roos, K. Andersson, *Chem. Phys. Lett.* **1995**, *245*, 215.
- [18] Y. Kitagawa, T. Saito, M. Ito, M. Shoji, K. Koizumi, *Chem. Phys. Lett.* **2007**, *442*, 445.
- [19] B. O. Roos, A. C. Borin, L. Gagliardi, *Angew. Chemie Int. Ed.* **2007**, *46*, 1469.
- [20] Y. Kurashige, T. Yanai, *J. Chem. Phys.* **2011**, *135*, 094104.
- [21] T. Muller, *J. Phys. Chem.* **2009**, *113*, 12729.
- [22] F. Ruipérez, F. Aquilante, J. M. Ugalde, I. Infante, *J. Chem. Theory Comput.* **2011**, *7*, 1640.
- [23] S. Vancoillie, P. A. Malmqvist, V. Veryazov, *J. Chem. Theory Comput.* **2016**, *12*, 1647.
- [24] Z. Luo, Y. Ma, X. Wang, H. Ma, *J. Chem. Theory Comput.* **2018**, *14*, 4747.
- [25] A. H. Pakiari, S. Shariati, *Comput. Theor. Chem.* **2016**, *1084*, 169.
- [26] Y. Yamada, K. Hongo, K. Egashira, Y. Kita, U. Nagashima, M. Tachikawa, *Chem. Phys. Lett.* **2013**, *555*, 84.
- [27] J. N. van Niekerk, F. R. L. Schoening, *Acta Crystallogr.* **1953**, *6*, 227.
- [28] F. Bertolotti, A. Forni, G. Gervasio, D. Maraballo, E. Diana, *Polyhedron* **2012**, *42*, 118.
- [29] R. D. Davy, M. B. D. Hall, *J. Am. Chem. Soc.* **1989**, *111*, 1268.
- [30] K. Andersson, C. W. Bauschlicher, B. J. Persson, B. O. Roos, *Chem. Phys. Lett.* **1996**, *257*, 238.
- [31] S. Petrie, R. Stranger, *Inorg. Chem.* **2004**, *43*, 2597.
- [32] L. Noodleman, J. G. J. Norman, *J. Chem. Phys.* **1979**, *70*, 4903.
- [33] F. A. Cotton, H. Chen, L. M. Daniels, X. Feng, *J. Am. Chem. Soc.* **1992**, *114*, 8980.

- [34] P. Huang, Y. Natori, Y. Kitagawa, Y. Sekine, W. Kosaka, H. Miyasaka, *Inorg. Chem.* **2018**, *57*, 5371.
- [35] J. N. van Niekerk, F. R. L. Schoening, J. F. de Wet, *Acta Crystallogr.* **1953**, *6*, 501.
- [36] F. A. Cotton, B. G. Deboer, M. D. Laprade, J. R. Pipal, D. A. O. Uci, *Acta Crystallogr. Sect. B Struct. Sci. Cryst. Eng. Mater.* **1971**, *27*, 1664.
- [37] S. N. Ketkar, M. Fink, *J. Am. Chem. Soc.* **1985**, *107*, 338.
- [38] M. Benard, P. Coppens, M. L. Delucia, E. D. Stevens, *Inorg. Chem.* **1980**, *19*, 1924.
- [39] R. Wiest, M. Benard, *Chem. Phys. Lett.* **1983**, *98*, 102.
- [40] R. A. Kok, M. B. D. Hall, *J. Am. Chem. Soc.* **1983**, *105*, 676.
- [41] R. A. Kok, M. B. D. Hall, *Inorg. Chem.* **1985**, *24*, 1542.
- [42] A. D. Becke, *Phys. Rev. A* **1988**, *38*, 3098.
- [43] C. Lee, W. Yang, R. G. Parr, *Phys. Rev. B* **1988**, *37*, 785.
- [44] A. D. Becke, *J. Chem. Phys.* **1993**, *98*, 5648.
- [45] S. H. Vosko, L. Wilk, M. Nusair, *Can. J. Phys.* **1980**, *58*, 1200.
- [46] S. Grimme, J. Antony, S. Ehrlich, H. Krieg, *J. Chem. Phys.* **2010**, *132*, 154104.
- [47] R. Krishnan, J. S. Binkley, R. Seeger, J. A. Pople, *J. Chem. Phys.* **1980**, *72*, 650.
- [48] A. D. McLean, G. S. Chandler, *J. Chem. Phys.* **1980**, *72*, 5639.
- [49] M. J. Frisch, G. W. Trucks, H. B. Schlegel, G. E. Scuseria, M. A. Robb, J. R. Cheeseman, G. Scalmani, V. Barone, G. A. Petersson, H. Nakatsuji, X. Li, M. Caricato, A. Marenich, J. Bloino, B. G. Janesko, R. Gomperts, B. Mennucci, H. P. Hratchian, J. V. Ortiz, A. F. Izmaylov, J. L. Sonnenberg, D. Williams-Young, F. Ding, F. Lipparini, F. Egidi, J. Goings, B. Peng, A. Hada, M. Ehara, K. Toyota, R. Fukuda, J. Hasegawa, M. Ishida, T. Nakajima, Y. Honda, O. Kitao, H. Nakai, T. Vreven, K. Throssell, J. A. Montgomery Jr., J. E. Peralta, F. Ogliaro, M. Bearpark, J. J. Heyd, E. Brothers, K. N. Kudin, V. N. Staroverov, T. Keith, R. Kobayashi, J. Normand, K. Raghavachari, A. Rendell, J. C. Burant, S. S. Iyengar, J. Tomasi, M. Cossi, J. M. Millam, M. Klene, C. Adamo, R. Cammi, J. W. Ochterski, R. L. Martin, K. Morokuma, O. Farkas, J. B. Foresman, D. J. Fox, Gaussian 09, Revision D.01. Gaussian, Inc., Wallingford CT, (2009).
- [50] S. Grimme, *J. Chem. Phys.* **2006**, *124*, 034108.
- [51] T. Schwabe, S. Grimme, *Phys. Chem. Chem. Phys.* **2006**, *8*, 4398.
- [52] F. Weigend, R. Ahlrichs, *Phys. Chem. Chem. Phys.* **2005**, *7*, 3297.
- [53] V. Bachler, G. Olbrich, F. Neese, K. Wieghardt, *Inorg. Chem.* **2002**, *41*, 4179.
- [54] D. Herebian, K. E. Wieghardt, F. Neese, *J. Am. Chem. Soc.* **2003**, *125*, 10997.
- [55] S. Blanchard, F. Neese, E. Bothe, E. Bill, T. Weyhermüller, K. Wieghardt, *Inorg. Chem.* **2005**, *44*, 3636.
- [56] K. Chłopek, E. Bothe, F. Neese, T. Weyhermüller, K. Wieghardt, *Inorg. Chem.* **2006**, *45*, 6298.
- [57] K. Chłopek, N. Muresan, F. Neese, K. Wieghardt, *Chem. A Eur. J.* **2007**, *13*, 8390.
- [58] R. Boča, Theoretical Foundations of Molecular Magnetism, Elsevier Science, Amsterdam, **1999**.
- [59] K. Yamaguchi, T. Tsunekawa, Y. Toyoda, T. Fueno, *Chem. Phys. Lett.* **1988**, *143*, 371.
- [60] R. Caballol, O. Castell, F. Illas, P. R. de Moreira, J.-P. Malrieu, *J. Phys. Chem. A* **1997**, *101*, 7860.
- [61] F. Neese, *J. Am. Chem. Soc.* **2006**, *128*, 10213.
- [62] S. Zein, F. Neese, *J. Phys. Chem. A* **2008**, *112*, 7976.
- [63] C. Duboc, D. Ganyushin, K. Sivalingam, M. N. Collomb, F. Neese, *J. Phys. Chem. A* **2010**, *114*, 10750.
- [64] F. Neese, *J. Comput. Chem.* **2003**, *24*, 1740.
- [65] F. Neese, *Wiley Interdiscip. Rev. Comput. Mol. Sci.* **2018**, *8*, 4.
- [66] C. Angeli, R. Cimraglia, S. Evangelisti, T. Leininger, J.-P. Malrieu, *J. Chem. Phys.* **2001**, *114*, 10252.
- [67] C. Angeli, R. Cimraglia, J.-P. Malrieu, *Chem. Phys. Lett.* **2001**, *350*, 297.
- [68] C. Angeli, S. Evangelisti, R. Cimraglia, D. Maynau, *J. Chem. Phys.* **2001**, *117*, 10525.
- [69] R. W. A. Havenith, P. R. Taylor, C. Angeli, R. Cimraglia, K. Ruud, *J. Chem. Phys.* **2004**, *120*, 4619.
- [70] R. Dovesi, A. Erba, R. Orlando, C. M. Zicovich-Wilson, B. Civalieri, L. Maschio, M. Rérat, S. Casassa, J. Baima, S. Salustro, B. Kirtman, *Wiley Interdiscip. Rev. Comput. Mol. Sci.* **2018**, *8*, 1.
- [71] R. Dovesi, V. R. Saunders, C. Roetti, R. Orlando, C. M. Zicovich-Wilson, F. Pascale, B. Civalieri, K. Doll, N. M. Harrison, I. J. Bush, Ph. D'Arco, M. Llunel, M. Causa, Y. Noel, L. Maschio, A. Erba, M. Rérat, S. Casassa, CRYSTAL17 User's Manual, University of Torino, Torino, **2017** (2017).
- [72] M. F. Peintinger, D. V. Oliveira, T. Bredow, *J. Comput. Chem.* **2013**, *34*, 451.
- [73] R. F. W. Bader, Atoms in Molecules: A Quantum Theory, Oxford University Press, Oxford, **1990**.
- [74] T. A. Keith, AIMAll, version 14.04.17, TK Gristmill Software, Overland Park, KS, **2014**. aim.tkgristmill.com.
- [75] Zou, W. Molden2AIM (Version 4.2.1), Xian, <https://github.com/zorkzou/Molden2AIM>. (2018).
- [76] C. Gatti, TOPOND-96: an electron density topological program for systems periodic in N (N=0–3) dimensions, User's manual, CNR-CSR SRC, Milano, **1996**.
- [77] A. D. Becke, K. E. Edgecombe, *J. Chem. Phys.* **1990**, *92*, 5397.
- [78] M. Kohout, A. V. Savin, *Int. J. Quantum Chem.* **1996**, *60*, 875.
- [79] Kohout, M. DGrid, Version 4.6, Radebeul, Dresden, (2011).
- [80] T. Lu, F. Chen, *J. Comput. Chem.* **2012**, *33*, 580.
- [81] A. M. K. Müller, *Phys. Lett. A* **1984**, *105*, 446.
- [82] E. Francisco, M. A. Blanco, Á. M. Martín Pendás, *J. Chem. Phys.* **2007**, *126*, 094102.
- [83] V. Bezugly, P. Wielgus, M. Kohout, F. R. Wagner, *J. Comp. Chem.* **2010**, *31*, 1504.
- [84] V. Bezugly, P. Wielgus, M. Kohout, F. R. Wagner, *J. Comp. Chem.* **2010**, *31*, 2273.
- [85] X. Fradera, M. A. Austen, R. F. W. Bader, *J. Phys. Chem. A* **1999**, *103*, 304.
- [86] P. Flükiger, H. P. Lüthi, S. Sortmann, J. Weber, MOLEKEL 4.3, Swiss Center for Scientific Computing, Manno, Switzerland, **2002**.
- [87] A. Kokalj, *J. Mol. Graph. Model.* **1999**, *17*, 176.
- [88] A. Kokalj, *Comput. Mater. Sci.* **2003**, *28*, 155.
- [89] R. F. W. Bader, M. E. Stephens, *J. Am. Chem. Soc.* **1975**, *97*, 7391.
- [90] A. A. Rykounov, A. I. Stash, V. V. Zhurov, E. A. Zhurova, A. A. Pinkerton, *Acta Crystallogr. Sect. B Struct. Sci. Cryst. Eng. Mater.* **2011**, *67*, 425.
- [91] R. Llusar, A. Beitrag, J. Andres, F. Fasteur, B. Silvi, *J. Phys. Chem. A* **2001**, *105*, 9460.
- [92] L. Veis, A. Antalík, J. Brabec, F. Neese, Ö. Legeza, J. Pittner, *J. Phys. Chem. Lett.* **2016**, *7*, 4072.
- [93] L. Freitag, S. Knecht, C. Angeli, M. Reiher, *J. Chem. Theory Comput.* **2017**, *13*, 451.
- [94] S. Guo, M. A. Watson, W. Hu, Q. Sun, G. K. Chan, *J. Chem. Theory Comput.* **2016**, *12*, 1583.
- [95] V. Pichon-Pesme, C. Lecomte, H. Lachekar, *J. Phys. Chem.* **1995**, *99*, 6242.
- [96] S. Domagala, C. Jelsch, *J. Appl. Cryst.* **2008**, *41*, 1140.
- [97] B. Dittich, T. Koritsánszky, P. Luger, *Angew. Chemie Int. Ed.* **2004**, *43*, 2718.
- [98] T. Koritsánszky, A. Volkov, P. Coppens, *Acta Crystallogr. Sect. A Found. Adv.* **2002**, *58*, 464.
- [99] B. Meyer, A. Genoni, *J. Phys. Chem. A* **2018**, *122*, 8965.

Received: 30 September 2019

Revised: 13 November 2019

Accepted: 13 November 2019

Published online on 5 December 2019